Resolving simulated sequences of earthquakes and fault interactions: implications for physics-based seismic hazard assessment

Valere Lambert[1] and Nadia Lapusta[1]

[1]California Institute of Technology

November 26, 2022

Abstract

Physics-based numerical modeling of earthquake source processes strives to predict quantities of interest for seismic hazard, such as the probability of an earthquake rupture jumping between fault segments. How to assess the predictive power of numerical models remains a topic of ongoing debate. Here, we investigate how sensitive are the outcomes of numerical simulations of sequences of earthquakes and aseismic slip to choices in numerical discretization and treatment of inertial effects, using a simplified 2-D crustal fault model with two co-planar segments separated by a creeping barrier. Our simulations demonstrate that simplifying inertial effects and using oversized cells significantly affects the resulting earthquake sequences, including the rate of two-segment ruptures. We find that a number of fault models with different properties and modeling assumptions can produce comparable frequency-magnitude statistics and static stress drops but have rates of two-segment ruptures ranging from 0 (single-segment ruptures only) to 1 (two-segment ruptures only). For sufficiently long faults, we find that long-term sequences of events can substantially differ even among simulations that are well-resolved by standard considerations. In such simulations, some outcomes, such as static stress drops, are stable among adequately-resolved simulations, whereas others, such as the rate of two-segment ruptures, can be highly sensitive to numerical procedures and physical assumptions, and hence cannot be reliably inferred. Our results emphasize the need to examine the potential dependence of simulation outcomes on the modeling procedures and resolution, particularly when assessing their predictive value for seismic hazard assessment.

Resolving simulated sequences of earthquakes and fault interactions: implications for physics-based seismic hazard assessment

Valère Lambert[1] **and Nadia Lapusta**[1,2]

[1]Seismological Laboratory, California Institute of Technology, Pasadena, California, USA

[2]Department of Mechanical and Civil Engineering, California Institute of Technology, Pasadena,

California, USA

Key Points:

- Long-term interactions of fault segments qualitatively differ among fully versus quasi-dynamic simulations, and when using oversized cells.
- Reproducing frequency-magnitude distributions and static stress drops is not sufficient to constrain the rate of multi-segment ruptures.
- Simulated earthquake sequences can differ due to compounded effects of numerical errors, even when individual ruptures are well-resolved.

Corresponding author: Valère Lambert, `vlambert@caltech.edu`

Abstract

Physics-based numerical modeling of earthquake source processes strives to predict quantities of interest for seismic hazard, such as the probability of an earthquake rupture jumping between fault segments. How to assess the predictive power of numerical models remains a topic of ongoing debate. Here, we investigate how sensitive are the outcomes of numerical simulations of sequences of earthquakes and aseismic slip to choices in numerical discretization and treatment of inertial effects, using a simplified 2-D crustal fault model with two co-planar segments separated by a creeping barrier. Our simulations demonstrate that simplifying inertial effects and using oversized cells significantly affects the resulting earthquake sequences, including the rate of two-segment ruptures. We find that a number of fault models with different properties and modeling assumptions can produce comparable frequency-magnitude statistics and static stress drops but have rates of two-segment ruptures ranging from 0 (single-segment ruptures only) to 1 (two-segment ruptures only). For sufficiently long faults, we find that long-term sequences of events can substantially differ even among simulations that are well-resolved by standard considerations. In such simulations, some outcomes, such as static stress drops, are stable among adequately-resolved simulations, whereas others, such as the rate of two-segment ruptures, can be highly sensitive to numerical procedures and physical assumptions, and hence cannot be reliably inferred. Our results emphasize the need to examine the potential dependence of simulation outcomes on the modeling procedures and resolution, particularly when assessing their predictive value for seismic hazard assessment.

1 Introduction

Earthquakes occur in the context of fault networks and many large earthquakes span several fault segments. This reality brings about the issue of fault interaction and highlights the need for simulating earthquake source processes over several fault segments and regional-scale fault networks. How dynamic ruptures navigate fault segmentation has strong implications for seismic hazard analysis (Field, 2019). Earthquakes are ca-

pable of jumping fault segments. For example, the 1992 Landers earthquake succeeded in rupturing across at least 4 fault segments, amounting to a Mw 7.3 event (Sieh et al., 1993). The 2016 Mw 7.8 Kaikoura earthquake ruptured at least 21 segments of the Marlborough fault system (Ulrich et al., 2019). Increasingly, seismological observations show that it is not uncommon to see ruptures navigating and triggering subsequent ruptures within fault networks, including the recent 2019 Mw 6.4 and 7.1 Ridgecrest earthquakes (Ross et al., 2019), and the 2012 Mw 8.6 and 8.2 Indian Ocean earthquakes (Wei et al., 2013), the largest and second-largest recorded strike-slip earthquakes to date. Yet, in any given seismogenic region, the record of past large events is not long enough to forecast the behavior of ruptures with respect to the existing fault segments, specifically how likely would the rupture be to jump between nearby segments, prompting the discussion on whether and how physics-based models may inform this and other questions important for seismic hazard assessment (Field, 2019).

Determining what conditions allow a dynamic rupture to propagate or arrest are key to understanding the maximum potential magnitude of an earthquake. Previous modeling of single fully dynamic ruptures have shown great success in investigating earthquake propagation in nonplanar and multi-segment fault models, including step-overs and branched geometries (Harris et al., 1991; Harris & Day, 1993, 1999; Kame et al., 2003; Duan & Oglesby, 2006; Dunham et al., 2011a; Galvez et al., 2014; Douilly et al., 2015; Lozos et al., 2015; Hu et al., 2016; Withers et al., 2018; Ando & Kaneko, 2018; Wollherr et al., 2019; Ulrich et al., 2019). In particular, such modeling has shown that the ability of a rupture to propagate across segments depends on the stresses before the rupture and shear resistance assumptions, as well as the geometry of the fault system. However, single-rupture simulations need to select initial conditions and need additional assumptions to incorporate the effect of previous seismic and aseismic slip.

Fault processes involve both sequences of dynamic events and complex patterns of quasi-static slip. Simulating this behavior in its entirety is a fascinating scientific prob-

lem. However, even for the more pragmatic goal of physics-based predictive modeling

of destructive large dynamic events, it is still important to consider sequences of earth-

quakes and aseismic slip (SEAS), since prior slip events, including aseismic slip, may de-

termine where earthquakes would nucleate as well as modify stress and other initial con-

ditions before dynamic rupture. Furthermore, such simulations provide a framework for

determining physical properties consistent with a range of observations including geode-

tically recorded surface motions, microseismicity, past (including paleoseismic) events,

and thermal constraints, and hence may inform us about the current state of a fault seg-

ment or system and potential future rupture scenarios (e.g. Lapusta et al., 2000; Lapusta

& Rice, 2003; Liu & Rice, 2005; Ben-Zion & Rice, 1997; Chen & Lapusta, 2009; Kaneko

et al., 2010; Segall et al., 2010; Barbot et al., 2012; Noda & Lapusta, 2013; Erickson &

Dunham, 2014; Erickson & Day, 2016; Jiang & Lapusta, 2016; Lambert & Barbot, 2016;

Allison & Dunham, 2018; Lin & Lapusta, 2018; Cattania, 2019; Perry et al., 2020; Lam-

bert et al., 2021). However, simulating long-term slip histories is quite challenging be-

cause of the variety of temporal and spatial scales involved.

Recently, several earthquake simulators have been developed with the goal of sim-

ulating millions of earthquake ruptures over regional fault networks for tens of thousands

of years (Tullis et al., 2012; Richards-Dinger & Dieterich, 2012; Shaw et al., 2018). The

term "simulators" typically refers to approaches that employ significant simplifications,

compared to most SEAS simulations, in solution procedures and physical processes, in

order to simulate earthquake sequences on complex, regional scale 3-D fault networks

for long periods of time. For example, earthquake simulators typically account only for

the quasi-static stress transfer due to earthquake events, ignoring wave-mediated stress

changes, aseismic slip/deformation, and fluid effects; employ approximate rule-based up-

date schemes for earthquake progression instead of solutions of the governing continuum

mechanics equations; and use oversized numerical cells. Such simplifications are currently

necessary to permit simulations of hundreds of thousands of events over hundreds of fault

segments that comprise the regional networks (Shaw et al., 2018). Earthquake simula-

tors have matched a number of regional-scale statistical relations, including the Gutenberg-Richter frequency-magnitude scaling (Shaw et al., 2018), and highlighted the importance of large-scale fault and rupture interactions.

Here, we examine the sensitivity of the long-term interaction of fault segments to choices in numerical discretization and representations of inertial effects in simulated sequences of earthquakes and aseismic slip, using a relatively simple 2-D model of two co-planar strike-slip fault segments separated by a velocity-strengthening (VS) barrier. We explore how considerations for adequate numerical resolution and convergence depend on the physical assumptions and complexity of earthquake sequences as well as on the modeling outcome of interest. We especially focus on the rate of earthquake ruptures jumping across the VS barrier and examine whether reproducing comparable earthquake frequency-magnitude statistics and static stress drops provides sufficient predictive power for the jump rate, a quantity of interest to seismic hazard studies (Field, 2019).

2 Model setup and numerical resolution

Our simulations are conducted following the methodological developments of Lapusta et al. (2000), Noda and Lapusta (2010) and Lambert et al. (2021). We consider a one-dimensional (1-D) fault embedded into a 2-D uniform, isotropic, elastic medium (Figure 1). The 2-D model approximates a faulted crustal plate coupled to a moving substrate using the idea of a constrained continuum (Lehner et al., 1981; Johnson, 1992). Fault slip may vary spatially along-strike but it is depth-averaged through a prescribed seismogenic thickness $\lambda_S = 15$ km, beneath which the elastic domain is coupled to a substrate moving at the prescribed loading rate ($V_{\mathrm{pl}} = 10^{-9}$ m/s). The elastodynamic equation for the depth-averaged displacement along-strike $\overline{u}(x, y, t)$ is given by (Lehner et al., 1981; Kaneko & Lapusta, 2008):

$$Z^2 \frac{\partial^2 \overline{u}}{\partial x^2} + \frac{\partial^2 \overline{u}}{\partial y^2} + \frac{1}{\lambda_{\mathrm{eff}}^2} \left(\frac{1}{2} \mathrm{sign}(y) V_{\mathrm{pl}} t - \overline{u} \right) = \frac{1}{c_s} \frac{\partial^2 \overline{u}}{\partial t^2}, \tag{1}$$

where $\lambda_{\text{eff}} = (\pi/4)\lambda_{\text{S}}$ and $Z = 1/(1 - \nu)$, with ν being the Poisson's ratio. The effective wave speed along-strike for the crustal plane model is $c_L = Zc_s$, where c_s is the shear wave speed. The along-strike slip is then given by $\delta(x,t) = \overline{u}(x, y = 0^+, t) - \overline{u}(x, y^-, t)$.

Our simulations resolve sequences of earthquakes and aseismic slip (SEAS) in their entirety, including the gradual development of frictional instability and spontaneous nucleation, dynamic rupture propagation, post-seismic slip that follows the event, and the interseismic period between events (Figure 2). In all models, frictional resistance along the fault interface is governed by the standard laboratory-derived rate-and-state friction law with the state evolution described by the aging law (Dieterich, 1979; Ruina, 1983):

$$\tau = \overline{\sigma}f = (\sigma - p)\left[f_* + a\ln\frac{V}{V_*} + b\ln\frac{V_*\theta}{D_{\text{RS}}}\right], \tag{2}$$

$$\frac{d\theta}{dt} = 1 - \frac{V\theta}{D_{\text{RS}}}, \tag{3}$$

where $\overline{\sigma} = (\sigma - p)$ is the effective normal stress, σ is the normal stress, p is the pore pressure, τ is the shear stress, f is the friction coefficient, V is the slip velocity, θ is the state variable, D_{RS} is the characteristic slip for the evolution of the state variable, f_* is the reference steady-state friction coefficient corresponding to a reference slip rate V_*, and a and b are the direct and evolution effect constitutive parameters, respectively.

At steady-state (constant slip velocity), the shear stress and state variable evolve to their steady-state values τ_{ss} and θ_{ss} given by:

$$\tau_{ss}(V) = (\sigma - p)\left[f_* + (a - b)\ln\frac{V}{V_*}\right], \tag{4}$$

$$\theta_{ss}(V) = \frac{D_{\text{RS}}}{V}. \tag{5}$$

128   The combination of frictional properties such that $(a - b) > 0$ results in steady-state

129   velocity-strengthening (VS) behavior, where the shear resistance increases with an in-

130   crease in slip velocity and where stable slip is expected. If $(a - b) < 0$ then the fault

131   exhibits velocity-weakening (VW) behavior, in which case an increase in slip velocity leads

132   to a decrease in shear resistance, making these regions of the fault potentially seismo-

133   genic if their size exceeds a critical nucleation size.

134   Two theoretical estimates of the nucleation size in mode II are (Rice & Ruina, 1983;

135   Rubin & Ampuero, 2005):

$$h^*_{RR} = \frac{\pi}{4} \frac{\mu L}{(1 - \nu)(b - a)(\sigma - p)}; \quad h^*_{RA} = \frac{2}{\pi} \frac{\mu L b}{(1 - \nu)(b - a)^2(\sigma - p)}, \quad (6)$$

136   where μ is the shear modulus. The estimate h^*_{RR} was derived from the linear stability

137   analysis of steady frictional sliding by Rice and Ruina (1983). It also represents the crit-

138   ical cell size for steady-state quasi-static sliding such that larger cells can become un-

139   stable on their own. Thus h^*_{RR} represents a key length scale to resolve for slow interseis-

140   mic processes and earthquake nucleation (Rice & Ruina, 1983; Lapusta et al., 2000). The

141   estimate h^*_{RA} was determined in the parameter regime $a/b > 0.5$ using the energy bal-

142   ance of a quasi-statically expanding crack (Rubin & Ampuero, 2005), and provides an

143   estimate of the minimum size for a slipping region that releases enough stored energy

144   to result in the radiation of waves.

145   We aim to explore the impact of numerical resolution on the long-term simulated

146   slip behavior of sequences of earthquakes and aseismic slip. The nucleation size, h^*, es-

147   timated by either h^*_{RR} or h^*_{RA} from equation (6), is one length-scale that clearly needs

148   to be well resolved. Early resolution studies for sequences of events showed that reso-

149   lution of the nucleation scale h^*_{RR} by 20 to 40 cells is required for stable numerical re-

150   sults (Lapusta et al., 2000). Later, the need to resolve the nucleation size by at least 20

151   cells was shown to be due to the more stringent criterion of resolving the region where

152   shear resistance breaks down at the rupture front, often referred to as the cohesive zone.

153   The cohesive zone can be an order of magnitude smaller than the nucleation size, depend-

154   ing on the constitutive description (Day et al., 2005; Lapusta & Liu, 2009). The size of

155   the cohesive zone depends on the weakening rate W of shear stress with slip associated

156   with the constitutive law. The quasi-static estimate Λ_0 of the cohesive zone size at near-

157   zero rupture speed and constant W is given by:

$$\Lambda_0 = C_1 \frac{\mu'}{W}, \tag{7}$$

158   where C_1 is a constant, $\mu' = \mu$ for mode III, and $\mu' = \mu/(1-\nu)$ for mode II (Rice,

159   1980). For standard rate-and-state friction with the aging form of the state variable evo-

160   lution, the weakening rate is given by $W = D_{\mathrm{RS}}/(b\overline{\sigma})$ (Lapusta & Liu, 2009) and:

$$\Lambda_0 = C_1 \frac{\mu' D_{\mathrm{RS}}}{b\overline{\sigma}}. \tag{8}$$

161   If one assumes that the traction distribution within the cohesive zone is linear, then the

162   constant C_1 can be approximated as $C_1 = 9\pi/32$ (Rice, 1980).

163   For fully dynamic rupture simulations, continuously resolving the breakdown pro-

164   cess at the rupture front becomes even more challenging as the cohesive zone size Λ ex-

165   hibits a contraction with increasing rupture speed v_R (e.g Rice, 1980):

$$\Lambda = \Lambda_0 A^{-1}(v_R); \quad A_{II}^{-1} = \frac{(1-\nu)c_s^2 \mathcal{D}}{v_R^2(1-v_R^2/c_s^2)^{1/2}}; \quad A_{III}^{-1} = (1-v_R^2/c_s^2)^{1/2}, \tag{9}$$

166   where $\mathcal{D} = 4(1-v_R^2/c_s^2)^{1/2}(1-v_R^2/c_p^2)^{1/2}-(2-v_R^2/c_s^2)^{1/2}$ with $c_p = \sqrt{2(1-\nu)/(1-2\nu)}c_s$.

167   Note that $A^{-1}(0^+) = 1$, giving the quasi-static cohesive zone estimate Λ_0 when $v_R =$

168   0^+. As the rupture speed approaches the limiting wave speed, $v_R \to c_R$ (Rayleigh wave

169   speed) for mode II and $v_R \to c_s$ (shear wave speed) for mode III, one has $A^{-1}(v_R) \to$

170   0 and the width of the breakdown region approaches zero. Hence it becomes increasingly

171   more challenging to resolve the rupture front during fully dynamic simulations if the rup-

¹⁷² ture accelerates towards the limiting speeds. Such acceleration typically occurs during

¹⁷³ long enough propagation of dynamic rupture over favorable prestress, unless impeded

¹⁷⁴ by additional factors such as unfavorable prestress or situations with increasing effec-

¹⁷⁵ tive breakdown energy, e.g., due to off-fault inelasticity, thermal pressurization of pore

¹⁷⁶ fluids, or navigating fault roughness (Poliakov et al., 2002; Andrews, 2005; Rice, 2006;

¹⁷⁷ Okubo et al., 2019; Dunham et al., 2011a; Perry et al., 2020; Lambert & Lapusta, 2020).

¹⁷⁸ Simulations of faults with rate-and-state friction and the aging form of the state vari-

¹⁷⁹ able evolution embedded in elastic bulk result in ruptures with near-constant breakdown

¹⁸⁰ energy (Perry et al., 2020) and this holds for most cases considered in this study. In sec-

¹⁸¹ tion 7, we show that adding an approximation of off-fault inelasticity to our simulations

¹⁸² that reduces the rupture speeds does not alter our conclusions.

¹⁸³ In our model, the fault contains a frictional domain consisting of two VW regions

¹⁸⁴ of length $\lambda_{VW} = 32$ km that are separated by a 2-km-long VS region that impedes rup-

¹⁸⁵ ture propagation. We select large enough values of the velocity strengthening in the cen-

¹⁸⁶ tral VS region so that the region acts like a barrier, requiring ruptures to jump/renucleate

¹⁸⁷ on the other side of the barrier to propagate over the second segment. This region is a

¹⁸⁸ proxy for what would be a gap in the fault connectivity, at least at the surface, requir-

¹⁸⁹ ing the ruptures to jump across. The remainder of the frictional region surrounding the

¹⁹⁰ VW segments has more mild VS properties (Figure 1). At the edges of the model, out-

¹⁹¹ side of the frictional domain, fault slip is prescribed at the loading plate rate. Values for

¹⁹² the model parameters used in our simulations are provided in Tables 1 and 2. We first

¹⁹³ examine models with lower instability ratio λ_{VW}/h_{RR}^* that result in quasi-periodic se-

¹⁹⁴ quences of events, and then consider models with higher instability ratios that result in

¹⁹⁵ more complex earthquake sequences and qualitatively different convergence behavior.

3 Resolving quasi-periodic fully dynamic sequences of earthquakes and aseismic slip (SEAS)

Let us consider the simulated slip behavior of fault model M1 with instability ratio $\lambda_{VW}/h_{RR}^* = 21$ (Table 2). Its quasi-static cohesive zone ($\Lambda_0 = 1.1$ km) should be well-resolved by cell sizes of 12.5 and 25 m, with 88 and 44 cells over Λ_0, respectively; the nucleation size is even larger and hence also well-resolved. Consistently with these considerations, these two well-discretized simulations produce the same relatively simple quasi-periodic sequences of earthquake events that periodically jump across the VS barrier (Figure 2A & B). We clearly see that the results are the same for the two simulations with different resolutions, including the local evolution of slip rate and shear stress during ruptures late in the earthquake sequence (Figure 2D-E). Note that the cohesive zone evolves throughout the rupture process, shrinking with the increasing rupture speed by 3-4 times in these simulations(Figure 2F-H) and the spatial discretization is fine enough to adequately characterize the rupture front throughout the entire dynamic process. Both simulations have the jump rate is 0.54; we define this rate of ruptures jumping across the VS barrier within a given time period as the total number of ruptures that propagate towards the barrier and result in seismic slip on both fault segments divided by the total number of ruptures that propagate towards the barrier.

The variability between different ruptures in fault model M1 is generally mild, as shown by their frequency-magnitude histograms (Figure 2C). To create the frequency-magnitude histograms, we compute the moment for each simulated event in our 2-D models as $M = \mu \bar{\delta} A$ where the rupture area is defined with respect to the rupture length L_R and seismogenic depth λ_S, as $A = (\pi/4)L_R^2$ when $L_R \leq \lambda_S$ and $A = L_R \lambda_S$ when $L_R > \lambda_S$.

The quasi-periodic nature of events observed over the first 4000 years in well-resolved simulations of fault model M1 persists in longer-duration simulations over 20,000 years, resulting in similar long-term jump rates of 0.48 to 0.54 depending on the time interval

223 considered (Figure 3). We also examine simulations of fault model M1 with different ini-

224 tial shear stress conditions and find that the long-term sequences of events converge to

225 the same quasi-periodic behavior upon adequate discretization, despite the initial few

226 events being different (Figure 3A vs B; details of initial shear stress distributions S1 and

227 S2 are provided in the Supplementary Materials). Simulations of fault model M1 thus

228 exhibit *long-term numerical convergence* upon adequate discretization, producing vir-

229 tually indistinguishable long-term slip behavior and a consistent rate of two-segment rup-

230 tures among simulations with differing initial conditions, after a sufficiently large initial

231 sequence of events.

232   Let us now consider simulations that use larger computational cells. The cell sizes

233 of 250 m and 125 m resolve the quasi-static cohesive zone Λ_0 with 4.5-9 cells (Figure 4).

234 While this resolution seems adequate (Day et al., 2005), one can anticipate that the dy-

235 namic shrinking of the cohesive zone size by 3-4 times would result in a more marginal

236 resolution of 1-3 cells. Indeed, we see that the simulated long-term sequences of events

237 and jump rates differ substantially from those of the well-resolved simulations (Figures

238 2A & B vs. 4A & B). Considering even larger cell sizes of 500 m and 1000 m brings fur-

239 ther differences in the event sequences and jump rates (Figure 5), with the earthquake

240 sequences that look plausible and not obviously numerically compromised even for the

241 largest cell sizes (Supplementary Figure S1). Note that the jump rate in simulations with

242 marginal and oversized cells is neither systematically larger nor smaller than the range

243 0.48-0.54 from the well-resolved cases, but varies from 0.25 to 0.95 depending on the choice

244 of numerical discretization.

245   Increasingly poor resolution of the dynamic cohesive zone at the rupture front and,

246 for the largest cell sizes, of the nucleation zone results in an increasing abundance of small

247 events (Figure 5), as had been shown in previous studies (Rice, 1993; Rice & Ben-Zion,

248 1996; Lapusta & Liu, 2009). Inadequate resolution of the dynamic rupture front prevents

249 simulating the actual stress concentration and promotes event arrest. Inadequate res-

olution of the nucleation size enables individual cells or small number of cells to fail independently due to the inadequate resolution of the stress interactions (Rice, 1993; Rice & Ben-Zion, 1996; Lapusta & Liu, 2009). Using sufficiently oversized cells can result in power-law statistics in terms of the frequency-magnitude distribution of simulated earthquake ruptures (Figure 5E-J; Rice, 1993; Rice & Ben-Zion, 1996).

Note that the suggested minimum average resolution of 3 cells of the (variable) cohesive zone from the dynamic rupture study by Day et al. (2005) is not adequate for convergent results in these earthquake sequence simulations. That criterion would be achieved in this model for a cell size between the 250 m and 125 m. Yet the simulated long-term behavior for those cell sizes is clearly different from the better-resolved and convergent results with the cell sizes of 25 m and 12.5 m. At the same time, the criterion by Day et al. (2005) works well for a single dynamic rupture as intended, since the first dynamic events in simulations with cell sizes 12.5 m, 25 m, 125 m, and 250 m are quite similar to each other (Supplementary Figure S2). The events are not identical, however; for example, the average slip with the resolution of 12.5 m and 125 m differs by 0.7%. Clearly, these differences - acceptable for a single event - accumulate in these highly nonlinear solutions, resulting in different event statistics and jump rate (Figure 5).

We find that our fully dynamic 2-D simulations of fault model M1, which include uniform VW properties with relatively mild weakening due to standard rate-and-state friction, converge when the quasi-static cohesive zone estimate Λ_0 is discretized by at least 22 cells, which translates to the average resolution of the dynamically variable cohesive zone size of 10-15 cells. Fault models with additional or different ingredients, such as fault heterogeneity/roughness, more efficient weakening, 3D elastodynamics with 3D faults, or different instability ratio, would require further considerations for resolution requirements that result in convergent simulations. For example, as we discuss in section 6, the convergence and resolution properties of models with higher instability ratios, which result in more complex earthquake sequences, are qualitatively different.

²⁷⁷   In the more complicated earthquake sequences observed in under-resolved simu-

²⁷⁸ lations of fault model M1, some statistics, such as the rate of two-segment ruptures, de-

²⁷⁹ pends on the specific period that one considers throughout the simulation. To explore

²⁸⁰ the variability in the event statistics and jump rate across the VS barrier in models with

²⁸¹ different numerical resolution, we examine the jump rate over different 2000-year peri-

²⁸² ods throughout longer term simulations of 20,000 years, using a sliding window of 1000

²⁸³ years starting at the beginning of the simulation (19 periods total; Figure 5). The choice

²⁸⁴ of a 2000-year period allows us to have a sufficient number (∼20) of large earthquakes

²⁸⁵ within a period to estimate jump rates. We also consider the outcomes for two differ-

²⁸⁶ ent initial conditions S1 and S2, as before. For the well-resolved simulations exhibiting

²⁸⁷ long-term convergence, the frequency-magnitude and 2000-year jump rate statistics for

²⁸⁸ simulations with different initiation conditions are comparable, with the jump rate for

²⁸⁹ all 2000-year periods being consistent with the overall 20,000 year jump rate (Figure 5A-

²⁹⁰ B). As the numerical resolution worsens, the sequences of events become more complex

²⁹¹ with greater variability in rupture sizes and increased production of smaller events (Fig-

²⁹² ure 5C-J). The jump rate during any 2000-year period also becomes more variable in marginally-

²⁹³ resolved simulations and can considerably differ from both the 20,000-year jump rate of

²⁹⁴ the same simulation as well as from the true jump rate in the well-resolved simulations.

²⁹⁵ Note that, despite being clearly affected by numerical resolution, the frequency-magnitude

²⁹⁶ and jump-rate distributions of inadequately resolved simulations can appear generally

²⁹⁷ consistent among simulations with similar cell sizes and different initial conditions (Fig-

²⁹⁸ ure 5 left vs. right columns). In other words, even if simulations using marginal or over-

²⁹⁹ sized cells produce comparable statistical properties for different initial conditions, these

³⁰⁰ characteristics do not necessarily represent robust features of the physical system but

³⁰¹ rather may still be numerical artifacts.

4 Interaction of fault segments in simulations with quasi-dynamic approximation for inertial effects

Many numerical studies of long-term fault behavior utilize quasi-dynamic solutions to the equations of motion, in which the wave-mediated stress transfers during the co-seismic phase are replaced with a radiation damping approximation (Rice, 1993). The quasi-dynamic approximation substantially reduces the computational expense of the simulation, as the consideration of stress redistribution by waves requires substantial additional storage and computational expense. Considerable insight into fault mechanics has been derived from studies using quasi-dynamic formulations, particularly when such approximations are used to incorporate new physical effects that may otherwise result in prohibitive computational expense, as well as in scenarios where it may be argued that inertial effects are relatively mild, such as during earthquake nucleation or during aseismic slip transients (Rice, 1993; Segall & Rice, 1995; Liu & Rice, 2005, 2007; Rubin & Ampuero, 2005; Segall et al., 2010; Liu, 2014; Lambert & Barbot, 2016; Erickson et al., 2017; Allison & Dunham, 2018). However, as with all approximations, it is important to be aware of how such simplifications modify the outcome of study (Thomas et al., 2014).

Let us review the quasi-dynamic approximation for inertial effects during sliding and study their implications for the long-term interaction of two fault segments. In the 2D boundary integral formulation, the elastodynamic shear stress along a 1D fault plane, can be expressed as (Cochard & Madariaga, 1994; Perrin et al., 1995):

$$\tau(x,t) = \tau^0(x,t) + \phi_{\text{static}}(x,t) + \phi_{\text{dynamic}}(x,t) - \eta V(x,t), \tag{10}$$

where $\tau^0(x,t)$ are the "loading" tractions (i.e. the stress induced on the fault plane if it were constrained against any slip), $\phi_{\text{static}}(x,t)$ and $\phi_{\text{dynamic}}(x,t)$ represent the static and dynamic contributions to the stress transfer along the fault, respectively, and the last term represents radiation damping ($\eta = \mu/(2c_s)$ for mode III).

326   The static solution for the equations of motion would only contain ϕ_{static}, which

327   depends only on the current values of slip along the fault. However, the static solution

328   does not exist during dynamic rupture when inertial effects becomes important. ϕ_{dynamic}

329   and ηV both arise due to the inertial effects. ϕ_{dynamic} represents the wave-mediated stress

330   interactions along the interface and this term is challenging to compute as it requires cal-

331   culating convolutions on time and storing the history of deformation. Radiation damp-

332   ing ηV is much easier to incorporate as it depends on the current slip rate, and repre-

333   sents part of the radiated energy (Rice, 1993). The quasi-dynamic approximation, in which

334   ϕ_{dynamic} is ignored and only ηV is included, allows the solution to exist during inertially-

335   controlled dynamic rupture. However, the solution is altered from the true elastodynamic

336   representation.

337   Let us consider the long-term behavior of fault model M1, as examined in section

338   3, but now using the quasi-dynamic approximation. For well-resolved quasi-dynamic sim-

339   ulations of fault model M1, we find that the long-term slip behavior of the two fault seg-

340   ment system is even simpler than for the fully dynamic case, with ruptures being exclu-

341   sively isolated to individual segments and the jump rate being zero (Figure 6A). For sim-

342   ulations with the increasing cell size, and thus decreasing spatial resolution, we see in-

343   creased variability in the size of the individual ruptures, to the point where some marginally-

344   resolved simulations produce ruptures that jump across the VS barrier, whereas well-

345   resolved simulations of the same fault model never do (Figure 6B-C). The increasing cell

346   size also leads to increased production of smaller events and more complicated fault be-

347   havior, similarly to the fully dynamic simulations (Figure 6D-F).

348   In addition to substantially reducing the computational expense associated with

349   calculating the wave-mediated stress transfers, quasi-dynamic simulations place milder

350   constraints on the spatial resolution since the cohesive zone always remains near the quasi-

351   static estimate, $\Lambda \approx \Lambda_0 = \Lambda(v_R = 0^+)$ (Figure 6G-H). This is because the stress trans-

352   fer calculated for the ruptures is always quasi-static, and the much stronger stress trans-

353   fer due to waves is ignored (Figure 7E). As a result, the quasi-dynamic simulations pro-

354   duce significantly smaller slip velocities and rupture speeds than the fully dynamic ones

355   7A-C, consistent with previous studies (Lapusta & Liu, 2009; Thomas et al., 2014).

356   One can attempt to enhance the slip rates and rupture speeds in the quasi-dynamic

357   simulations by reducing the radiation damping term η; this can be interpreted as increas-

358   ing the effective shear wave speed in the radiation damping term $c_s^{\text{enh.}} = \beta c_s$, thus al-

359   lowing for higher slip rates (Lapusta & Liu, 2009). We compare the enhanced quasi-dynamic

360   simulations ($\beta = 3$) with the standard quasi-dynamic ($\beta = 1$) and fully dynamic sim-

361   ulations of fault model M1 (Figure 8). Decreasing the radiation damping increases the

362   effective rupture speed and slip rate (Figure 7A -C) in comparison to the standard quasi-

363   dynamic simulation, however, for the parameters considered, it does not substantially

364   alter the long-term interactions of the two fault segments, nor match the rate of ruptures

365   jumping across the VS barrier in the fully dynamic case (Figure 8).

366   In comparing the three simulations with different treatment of the inertial effects,

367   it is clear that the fully dynamic ruptures result in higher slip rates and narrowing of

368   the cohesive zone (Figure 7). For simulations with standard rate-and-state friction, the

369   peak shear stresses vary mildly from fully dynamic versus quasi-dynamic representations,

370   as they are limited by the shear resistance of the fault, which has a relatively mild log-

371   arithmic dependence on slip rate. However, the stress transfer along the fault substan-

372   tially differs for fully dynamic versus quasi-dynamic representations (Figure 7E). The

373   difference between the stress transfer term and the shear stress is accommodated by the

374   radiation damping ηV, which results in higher slip rates V to balance the larger dynamic

375   stress stranfers (Figure 7C - E). Hence while the resolved peak shear stresses along the

376   fault may be comparable due to the specific choice of the constitutive relationship, the

377   rupture dynamics and kinematics, as seen through the stress transfer, slip rate, and rup-

378   ture speed along the fault, differ considerably with and without the inclusion of full in-

379   ertial effects.

These larger dynamic stress transfers facilitate the triggering and continued propagation of slip on the neighboring fault segment, rather than leaving the rupture to always be arrested by the creeping barrier, as in the well-resolved quasi-dynamic simulations (Figure 8). Decreasing the radiation damping term allows for somewhat higher slip rates and arbitrarily higher rupture speeds, but it does not mimic the full effects in the dynamic stress transfer, particularly at the rupture front. As the result, the fully dynamic simulations have higher jump rates. The differences between fully dynamic and quasi-dynamic approximations can be even more substantial for models with enhanced weakening at seismic slip rates from the flash heating of contact asperities or the thermal pressurization of pore fluids (Thomas et al., 2014).

5 Constraining rupture jump rates using earthquake frequency-magnitude statistics

Two common observations about natural earthquakes and regional seismicity are the average static stress drops between 1 to 10 MPa independently of the event magnitude (e.g Allmann & Shearer, 2009; Ye et al., 2016) as well as the frequency-magnitude statistics of earthquakes within a region, which commonly follow the Gutenberg-Richter power law relation (Field et al., 2013). Earthquake simulators are capable of matching these observations (Shaw et al., 2018). An important question is whether matching these constraints endows simulators with predictive power for other quantities of interest to seismic hazard assessment, such as the probability of multiple fault-segment ruptures, despite using approximations for inertial effects and oversized computational cells.

Let us consider this question using simulations of earthquake sequences in five fault models with the same fault geometry but different friction properties and different assumptions about inertial effects, and one additional model in which the effective seismogenic depth λ_S is slightly reduced from 15 to 14 km (Figure 9, Table 2). All six models have comparable nucleation and quasi-static cohesive zone sizes (Table 2) and use over-

406 sized cells of $\Delta x = 1000$ m (An example of well-resolved simulations with similar con-

407 clusions is given in section 7). The six simulations produce comparable frequency-magnitude

408 distributions, characterized by a b-value of 0.3-0.4 for 4000 years of the simulated time.

409 All six simulations also produce ruptures with comparable average static stress drops (Sup-

410 plementary Figure S3), with values typically between 1 and 10 MPa, as commonly in-

411 ferred for natural earthquakes (Allmann & Shearer, 2009; Ye et al., 2016).

412 However, the probability of a rupture jumping across the VS barrier varies dramat-

413 ically among the six simulations, ranging from 0 to near 100%. This substantial variabil-

414 ity in jump rate for simulations with comparable frequency-magnitude statistics persists

415 in longer-duration simulations over 20,000 years, where both the 20,000-year jump rate

416 and distributions of jump rates within individual 2000-year periods can substantially dif-

417 fer (Figure 10). In particular, fault model M1 results in a jump rate of 0 for the quasi-

418 dynamic simulation and near 1 for the fully dynamic simulation (Figures 9 and 10A vs.

419 D), despite having similar frequency-magnitude statistics. This case illustrates how us-

420 ing approximations for inertial effects may considerably bias estimates of the actual rate

421 of multi-segment ruptures, even if the frequency-magnitude statistics and static stress

422 drops are comparable. In addition, the suite of simulations suggest that the probabil-

423 ity of ruptures jumping across the VS barrier is sensitive to variations in the frictional

424 parameters, effective normal stress, as well as minor changes in the seismogenic depth.

425 The results from our simple 2-D modeling suggest that reproducing static stress

426 drops and frequency-magnitude statistics does not provide substantial predictive power

427 for the long-term interaction of fault segments. These results are perhaps not surpris-

428 ing given that many combinations of rate-and-state properties and effective normal stress

429 may produce ruptures with comparable static stress changes (Supplementary Figure S3),

430 but different overall levels of shear resistance. Moreover, numerical studies have shown

431 that fault models including enhanced dynamic weakening may also produce nearly magnitude-

432 invariant static stress drops with reasonable values between 1 - 10 MPa (Perry et al., 2020).

Such models with enhanced weakening result in larger dynamic stress variations which may mediate longer-range interactions among faults. However, enhanced weakening can also draw the average stress along the fault further away from nucleation conditions (Jiang & Lapusta, 2016; Lambert et al., 2021), which may produce less favorable conditions for dynamic triggering (Ulrich et al., 2019).

Similarly, a number of studies have demonstrated that power-law frequency-magnitude statistics can be reproduced in many models, including discrete fault models (Burridge & Knopoff, 1967; Bak & Tang, 1989; Olami et al., 1992), continuum fault models that are inadequately resolved and therefore numerically discrete (Ben-Zion & Rice, 1995), and continuum models with larger instability ratio (Wu & Chen, 2014; Cattania, 2019). In other words, Gutenberg-Richter statistics is consistent with a model having many potential rupture sizes, such as many individual faults of varying size or even a single fault that can host earthquakes of many sizes, between the nucleation size and fault dimensions. Therefore Gutenberg-Richter statistics may be compatible with a range of fault and/or fault network properties, and may not pose a considerable physical constraint on its own.

6 Resolution and convergence of SEAS simulations of faults with higher instability ratios

As discussed in section 3, we find that the discretization required to achieve long-term numerical convergence in simulations of fault model M1, with instability ratio of $\lambda_{VW}/h^*_{RR} \approx 21$, is more stringent than the current standards based on simulations of single dynamic ruptures and shorter SEAS simulations with lower instability ratios (Day et al., 2005; Lapusta & Liu, 2009). It has been demonstrated that fault models with relatively low instability ratios can result in quasi-periodic behavior, as seen in fault model M1 (Figure 2), whereas increasing the instability ratio can lead to more variable sequences of events with partial-segment ruptures of different rupture size, potentially consistent

459   with Gutenberg-Richter scaling (e.g Lapusta et al., 2000; Lapusta & Rice, 2003; Wu &

460   Chen, 2014; Michel et al., 2017; Cattania, 2019). As simulations with higher instabil-

461   ity ratios can produce ruptures with a wider variety of rupture sizes, with the rupture

462   size depending on the prestress conditions before rupture nucleation, one could hypoth-

463   esize that simulations of fault models with higher instability ratios may be more sensi-

464   tive to how the evolution of shear stress is resolved over long-term fault behavior.

465   To test that, let us consider sequences of events in fault model M5 (Table 2), which

466   has smaller characteristic slip distance, hence smaller nucleation size ($h_{RR}^* \approx 603$ m),

467   and larger instability ratio ($\lambda_{VW}/h_{RR}^* = 53$ vs. 21 in M1). Interestingly, we find that

468   the long-term sequence of simulated events in this model is not the same for finely-discretized

469   simulations with cell sizes of 25, 12.5 and 6.25 m (Figure 11), in which the quasi-static

470   cohesive zone Λ_0 is resolved by 18, 36 and 72 cells, respectively. The simulations pro-

471   duce nearly identical fault behavior for the first several hundred years of simulated time,

472   but then eventually begin to differ (Figure 11A-C).

473   Let us consider the first event in the three simulations of model M5 with fine dis-

474   cretization (Figure 11A-C), which all have the same initial conditions. If we examine the

475   local evolution of shear stress vs. slip at two spatial points in the simulations, the results

476   are virtually identical (Figure 12A-B), suggesting that a single dynamic rupture in these

477   finely-discretized simulations is adequately resolved. The evolution of shear stress and

478   slip rate at the rupture front with time is also well-resolved for each individual simula-

479   tion. While the different spatial resolutions result in small variations in the timing and

480   magnitude of the resolved properties at specified locations (Figure 12C-F), these differ-

481   ences are well within of what is considered well-resolved and convergent in prior stud-

482   ies (e.g Day et al., 2005). Early in the rupture, shortly after nucleation (near $x = 30$

483   km), the rupture front is almost identical in the three simulations. (Figure 12C & E).

484   As the rupture continues, small numerical differences for different resolutions result in

485   minor differences in the rupture, such as less than 0.08% difference in the rupture ar-

rival time and 2% difference in the peak slip rate between the two best-resolved simulations at the location close to the end of the rupture (Figure 12D & F). Such minor differences arise even for fine resolutions due to cumulative effects of slightly different representations of the solution by the discrete cells; for example, the fixed computational cells sample slightly different portions of the passing rupture front, leading to small accumulating differences in the magnitude of the shear stress and slip rate.

These small differences - that do not substantially alter the resulting rupture characteristics of individual events - do eventually alter the resulting earthquake sequences. For several ruptures early on in finely-discretized simulations, the slip and shear stress distributions before and after individual events are virtually indistinguishable (Figure 13A-B). However, eventually the small variations accumulate, resulting in enough differences in prestress conditions to cause more substantial differences in rupture lengths and amounts of slip within individual events, as well as changes in timing and location of earthquake nucleations (Figure 13C-E). As a result, the long-term history of sequences of slip events is altered (Figure 13F), including the rate of ruptures that jump across the VS barrier. We hypothesize that this alteration occurs for higher but not lower instability ratios due to more complex earthquake sequences in the latter case, although this issue requires further study.

Despite the specific sequences of events being different in the finely-discretized simulations shown in Figure 11A-C, we do find that certain outcomes are quite similar between these simulations, such as relationships between average static stress drop and seismic moment, average slip and rupture length, and breakdown energy and average slip, as well as general characteristics of the evolution of average shear stress and shear heating with time (Figure 14). Other parameters, such as the rate of ruptures jumping from one fault segment to another, are sensitive to numerical resolution even in these finely-resolved simulations, although they have relatively similar values (from 0.64 to 0.78). This highlights how the criteria for adequate discretization in numerical simulations can de-

pend on both the physical problem being considered and the outcome of interest. Note that while it is plausible that further discretization of fault model M5 would result in eventual convergence, and thus potentially a true rate of two-segment ruptures, the spatial discretization considered in this study is already much finer than those considered in most numerical SEAS studies, especially in more realistic models of 2D faults in 3D media which are often challenged to resolve Λ_0 by even 3 cells.

While the specific rate of ruptures jumping across the VS barrier varies among these finely-discretized simulations of fault model M5, it is possible that some broader statistical features of the jump rate are more robust. We examine the frequency-magnitude and 2000-year jump rate statistics for the long-term sequences of events in simulations of model M5 with different discretization. While the distributions mildly vary among finely-discretized simulations with differing cell sizes (12.5 m and 25 m), they are comparable (Figure 15 and Supplementary Figure S4). Thus, one can ascertain information about the probability distribution for the rate of multi-segment ruptures, even if specific results vary due to numerical discretization. Such small numerical perturbations could potentially be considered representative of various sources of physical perturbations on natural faults, and the statistical consistency of the distributions could be explored by producing ensembles of simulations with varying initial conditions. However, our results suggest that it is still important to sufficiently resolve the rupture process as the statistical distributions for rupture properties in simulations using oversized cells can be more substantially impacted by numerical artifacts and considerably vary from simulations with finer discretization (Figures 15 and 16).

7 Resolution and convergence in SEAS simulations with moderate rupture speeds due to an approximation for off-fault plasticity

While the 2-D fault models discussed in this study can be considered relatively simple, in some ways they can be particularly challenging to resolve. In fault models with

539 purely elastic bulk, dynamic ruptures are able to accelerate to rupture speeds close to

540 the limiting values c_L (e.g. Figure 7 for fault model M1), making it difficult to resolve

541 the significantly shrinking cohesive zone Λ. For example, during fully dynamic ruptures

542 in simulations of fault model M5, the rupture speed approaches $0.99c_L$ and the cohesive

543 zone shrinks more than 7 times to about 63.5 m. In real rocks, high slip rates and hence

544 high strain rates associated with dynamic rupture would be mitigated by off-fault inelas-

545 tic behavior around the rupture front, which would contribute to limiting the rupture

546 speed (Andrews, 2004; Dunham et al., 2011b).

547   In order to examine how conditions for resolution and convergence may differ in

548 long-term SEAS simulations with more moderate rupture speeds, we approximate the

549 effects of off-fault yielding by employing a limit on the slip velocity, as suggested by Andrews

550 (2004) and discussed in detail in Lambert et al. (2021). We consider long-term fully dy-

551 namic simulations of fault model M5 with the slip velocity limited to 2 m/s in order to

552 maintain rupture speeds around $0.8c_L$, consistent with the cohesive zone shrinking by

553 about a factor of 2 from the quasi-static estimate.

554   Surprisingly, the finely-discretized simulations of fault model M5 with limited rup-

555 ture speed still produce differing sequences of events, despite the rupture front and lo-

556 cal behavior being well-resolved and nearly identical for cell sizes of 6.25 to 25 m (Fig-

557 ure 17 and Supplementary Figure S5). As with the standard fully dynamic simulations

558 without the plasticity approximation, well-resolved simulations of fault model M5 with

559 the velocity limit are nearly identical for the initial few sequences (Figure 18A-B). How-

560 ever, the sequences of events begin to differ due to slight differences in how the evolu-

561 tion of shear stress is resolved during a slow-slip transient within the nucleation region

562 of an impending rupture, resulting in a 3-year delay between the nucleation of the sub-

563 sequent rupture in each simulation (Figure 18C-D). As discussed earlier for the standard

564 fully dynamic simulations, the small differences in prestress lead to mild differences in

565 slip and rupture size in subsequent events, which eventually compound to produce more

566 substantial variations in the long-term sequences of events (Figure 18 E-H). These re-

567 sults once again illustrate the extreme sensitivity of the long-term sequences of events,

568 and rates of two-segment ruptures, in this highly nonlinear problem, as well as the sig-

569 nificance of resolving how aseismic processes load, relax, and redistribute stress along

570 faults.

571 Interestingly, we see similar lack of convergence in quasi-dynamic simulations of

572 fault model M5, where long-term sequences, including the rate of two-segment ruptures,

573 differ in seemingly well-resolved simulations due to the compounded effects of small nu-

574 merical differences (Supplementary Figures S6 and 7). Moreover, despite the rupture front

575 being better resolved in the quasi-dynamic simulations and in fully dynamic simulations

576 withthe plasticity approximation than in the standard fully dynamic simulations, the se-

577 quences of events begin to diverge earlier. Specifically, while the standard fully dynamic

578 simulations of fault model M5 with cell sizes of $\Delta x = 6.25$ and $\Delta x = 12.5$ m have the

579 same event sequences through approximately 600 to 700 years of simulated time, fully

580 dynamic simulations with the plasticity approximation begin to substantially differ be-

581 tween 200 to 300 years, and quasi-dynamic simulations begin to noticeably differ between

582 100 to 200 years.

583 A potential explanation for this finding is that both the quasi-dynamic approxi-

584 mation and strong limitation on slip rate for fully dynamic simulations also limit the mag-

585 nitude of the stress transfer along the fault (Supplementary Figure S8), making the sim-

586 ulations more sensitive to small numerical differences. Thus, while the lower stress con-

587 centrations in both cases facilitate maintaining slower ruptures and resolving the break-

588 down of shear resistance at the rupture front, the smaller magnitudes for the stress trans-

589 fer along the fault makes rupture propagation more sensitive to variations in the pre-existing

590 shear stress ahead of the rupture front. Note that while the approximation for off-fault

591 plasticity substantially limits the peak slip rate and magnitude of the stress transfer along

592 the fault, the overall stress transfer for the fully dynamic rupture including the plastic-

ity approximation is still more pronounced than that of the quasi-dynamic ruptures, and remains more pronounced well behind the rupture front due to the continued arrival of waves from ongoing slip in already-ruptured regions. Both the quasi-dynamic simulations and the fully dynamic simulations with the plasticity approximation produce comparable static stress drops and frequency-magnitude statistics to the standard fully dynamic simulations (Supplementary Figures S4, 6 and 9). However, the rupture speeds and rates of two-segment ruptures are consistently higher for the fully dynamic simulations due to the substantially larger stress transfer. These results emphasize the significance of inertial effects when considering how ruptures navigate various forms of fault heterogeneity.

The simulations of model M5, without and with the plasticity approximation, provide another example of how earthquake sequences with similar frequency-magnitude statistics can result in different jump rates across the velocity-strengthening barrier. While the simulations with cell sizes of 6.25, 12.5, and 25 m have well-resolved cohesive zones (Figures 11 and 17) and similar event statistics (Supplementary Figures S4 and S9), they have jump rates ranging from 0.7-0.8 without the plasticity approximation to 0.3-0.5 with the plasticity approximation (Figures 11 and 17).

8 Conclusions and Discussion

We have investigated the sensitivity of numerical simulations of long-term sequences of earthquakes and aseismic slip (SEAS) to numerical discretization and treatment of inertial effects, using a simplified 2-D model of a 1D fault with two co-planar seismogenic, VW segments separated by a VS barrier. Our focus is, in part, on the resulting rate of rupture jumps across the barrier.

We find that the convergence of long-term simulated earthquake sequences with increasing numerical resolution may not always be achievable. Even if simulations are sufficiently discretized to produce consistent modeling results for individual ruptures or

short sequences of events, they may still produce different long-term sequences due to compounded effects of small numerical differences over many events. We have achieved the convergence for fault models with lower instability ratios λ_{VW}/h_{RR}^*, i.e., lower fault lengths in comparison to the nucleation size (Figure 3). In contrast, models with higher instability ratios exhibit different long-term behavior even in simulations that are well discretized by standard metrics (Day et al., 2005; Lapusta & Liu, 2009), including different specific sequences of earthquakes and different probability of ruptures jumping across the VS barrier. In the cases with convergent long-term behavior, the criteria for numerical resolution that leads to the same evolution of slip are more stringent than those for individual dynamic ruptures, i.e., the dynamic cohesive zone size needs to be discretized by more cells.

Our results show that numerical convergence in SEAS simulations depends not only on how well important length-scales are discretized but also on the sensitivity of the specific physical problem to small numerical perturbations. In particular, our results suggest that faults with higher instability ratios are more sensitive to accumulating numerical perturbations (Figure 19), although that conclusion requires further study. In another example, while quasi-dynamic simulations are easier to resolve and thus should result in smaller numerical discrepancies for sufficiently small cell sizes, the milder stress transfer compared to fully dynamic ruptures can make long-term quasi-dynamic simulations more sensitive to small perturbations in shear stress, as occurs in fault model M5. Hence empirical discretization criteria, such as those of (Day et al., 2005), should be seen as guidelines that may not be universally applicable to all physical models and outcomes of interest. Moreover, for some models, numerical convergence of long-term slip may not be possible, though statistical consistency may hold for some modeling results but not others (Figure 19). Overall, these findings highlight the importance for individual numerical studies to examine the sensitivity of their outcomes of interest to the choice of their numerical procedure and discretization.

For the fault models considered, we find that the rate of earthquake ruptures jumping across a VS barrier is sensitive to the numerical resolution, representation of inertial effects, as well as minor changes in physical properties, such frictional parameters, confining stress, seismogenic depth, and barrier size. This suggests that, even in this relatively simple model, the rate of ruptures jumping across a VS barrier is not a stable outcome that can always be reliably estimated from numerical models, unless the barrier is so large or small that the rate is reliably zero or 1 (Figure 20). The sensitivity of rupture jump rates to small changes in models suggests that the jump rates across barriers that serve as earthquake gates may also be highly sensitive to small physical perturbations on natural faults, and thus may be impractical to estimate in a reliable manner.

However, even for the models that do not achieve deterministic convergence with finer resolution, we find that some characteristics of well-resolved simulations are preserved, qualitatively and quantitatively. The characteristics include ranges of average source properties such as the average static stress drop, quantities related to energy partitioning such as the average breakdown energy, as well as general features of the average shear stress and shear heating evolution throughout time (Figure 14). These results suggest that some aspects of physical systems may be reliably determined from a given physics-based model, while others perhaps cannot, in the sense that they are very sensitive to numerical procedures and initial conditions, and even well-resolved models produce different outcomes with respect to those quantities. Our findings also suggest that it may be possible to discern some statistical aspects of the probability distribution for multi-segment ruptures from well-formulated numerical models, even if they do not exhibit convergence of long-term behavior with numerical resolution. However, as the jump rate appears to be sensitive to small perturbations in numerical and physical properties, it would be prudent to examine the statistical consistency of the jump rate distribution through large ensembles of models. Another route for examining plausible rupture scenarios for large earthquakes navigating key sections of fault networks would be to study detailed

674 dynamic rupture simulations that can handle more realistic fault geometries with full

675 treatment of inertial effects (e.g Wollherr et al., 2019; Ulrich et al., 2019), and produce

676 large ensembles of dynamic rupture scenarios with variations in initial conditions inspired

677 by SEAS simulations.

678 Our results confirm that quasi-dynamic simulations that ignore wave-mediated stress

679 transfer during dynamic rupture can lead to qualitative differences in the resolved rup-

680 ture behavior and long-term sequences of slip events. The wave-mediated stress redis-

681 tribution not only facilitates long-range interactions among portions of a fault and neigh-

682 boring segments, but also alters the state of stress at the rupture front, promoting higher

683 slip rates and more focused stress concentrations. In particular, the relatively small static

684 stress transfer in quasi-dynamic simulations makes the rupture front more susceptible

685 to unfavorable conditions, such as those one may expect from frictional heterogeneity,

686 fault roughness, and regions of unfavorably low prestress. In contrast, the larger wave-

687 mediated dynamic stresses in fully dynamic ruptures may assist rupture propagation in

688 navigating unfavorable fault conditions and geometric irregularities (Harris et al., 1991;

689 Harris & Day, 1993, 1999; Kame et al., 2003; Duan & Oglesby, 2006; Dunham et al., 2011a;

690 Galvez et al., 2014; Thomas et al., 2014; Douilly et al., 2015; Lozos et al., 2015; With-

691 ers et al., 2018; Ando & Kaneko, 2018; Wollherr et al., 2019; Ulrich et al., 2019). More-

692 over, the spatial pattern for dynamic stresses, which affects the preferential direction for

693 ruptures to branch or jump to neighboring faults, rotates as a function of the rupture

694 speed, and hence can be considerably different from a quasi-dynamic rupture (Kame et

695 al., 2003). Thus, considering full inertial effects during individual dynamic ruptures and

696 long-term sequences of slip events is particularly important when considering the inter-

697 action of multiple fault segments and the likelihood of ruptures propagating through po-

698 tentially unfavorable conditions.

699 Our results also confirm that using increasingly oversized cells, with or without wave-

700 mediated stress transfers, results in a progressively more complex slip response, with broader

distributions of event sizes, consistent with conclusions from prior studies (Ben-Zion & Rice, 1995). Using oversized cells and/or ignoring wave-mediated stress transfer significantly modifies the probability of two-segment ruptures, as well as the resulting earthquakes sequences.

Finally, we have examined whether the rate of ruptures jumping between two fault segments can be determined from simulations that reproduce frequency-magnitude statistics and average static stress drops (Shaw et al., 2018; Field, 2019). We find that these observations do not constrain rupture jump rates in our models. This highlights the need to better understand which field observations constrain long-term fault behavior, and thus provide predictive power for potential future hazards. Physics-based modeling is generally well-suited to explore these problems, where the relative contribution of physical mechanisms can be explored for a range of parameters, and intuition can be developed for the relationship among varying observational constraints and source characteristics. Note that a number of physical properties not included in our simplified 2-D models may qualitatively alter the behavior and hence interaction of neighboring fault segments, such as the explicit consideration of depth variations in slip and the depth extent to which ruptures propagate (e.g Jiang & Lapusta, 2016; Wollherr et al., 2019; Ulrich et al., 2019), time-dependent variations in loading from distributed deformation at depth (Lambert & Barbot, 2016; Allison & Dunham, 2018), and enhanced dynamic weakening at seismic slip rates (Tullis, 2007; Di Toro et al., 2011; Dunham et al., 2011a; Noda & Lapusta, 2013; Perry et al., 2020; Lambert et al., 2021). These are just a few physical ingredients that merit detailed study in the long-term interaction of fault segments.

Our results emphasize the need to examine the potential model dependence of simulation outcomes, including to numerical resolution, particularly when assessing their predictive value for seismic hazard assessment. Community initiatives, such as the Southern California Earthquake Center (SCEC) code comparisons for dynamic rupture simulations and simulations of sequences of seismic and aseismic slip (Harris et al., 2009;

728 Barall & Harris, 2014; Harris et al., 2018; Erickson et al., 2020), can provide further in-

729 sight into how numerically-derived results for different physical quantities may depend

730 on numerical methodologies and computational practices. The significant sensitivity of

731 the rate of multi-segment ruptures to small changes in numerical models implies that such

732 hazard parameters may also be sensitive to physical perturbations on natural faults. This

733 consideration motivates further evaluation of meaningful metrics for describing long-term

734 fault behavior and assessing seismic hazard, tasks for which physics-based modeling is

735 well-suited.

Parameter	Symbol	Value
Loading slip rate	V_{pl}	10^{-9} m/s
Shear wave speed	c_s	3299 m/s
Shear modulus	μ	36 GPa
Poisson's ratio	ν	0.25
Rate-and-state parameters		
Reference friction coefficient	f_*	0.6
Reference slip velocity	V_*	10^{-6} m/s
Direct effect (VS)	a_{VS}	0.02
Evolution effect (VS)	b_{VS}	0.003
Direct effect (barrier)	a_B	0.05
Evolution effect (barrier)	b_B	0.001
Length scales		
Fault length	λ	280 km
Frictional domain	λ_{fr}	258 km
Each VW segment	λ_{VW}	32 km
VS Barrier	λ_B	2 km
Seismogenic depth	λ_S	15 km

Table 1. Parameter values that are the same in different fault models unless specified otherwise

Parameter	Symbol	M1	M2	M3	M4	M5
Effective normal stress	$\overline{\sigma} = (\sigma - p)$	50 MPa	60 MPa	40 MPa	30 MPa	50 MPa
Characteristic slip	D_{RS}	20 mm	20 mm	20 mm	18 mm	8 mm
Direct effect (VW)	a_{VW}	0.005	0.005	0.005	0.005	0.005
Evolution effect (VW)	b_{VW}	0.015	0.0135	0.0175	0.02	0.015
Length scales						
Quasi-static cohesive zone	Λ_0	1.1 km	1.0 km	1.2 km	1.3 km	452 m
Nucleation size (R.&A., 2005)	h_{RA}^*	1.8 km	1.9 km	1.7 km	1.6 km	733 m
Nucleation size (R.&R., 1983)	h_{RR}^*	1.5 km	1.5 km	1.5 km	1.6 km	603 m
Instability ratio	λ_{VW}/h_{RA}^*	18	17	19	20	44
Instability ratio	λ_{VW}/h_{RR}^*	21	22	21	21	53

Table 2. Parameters values that vary among fault models
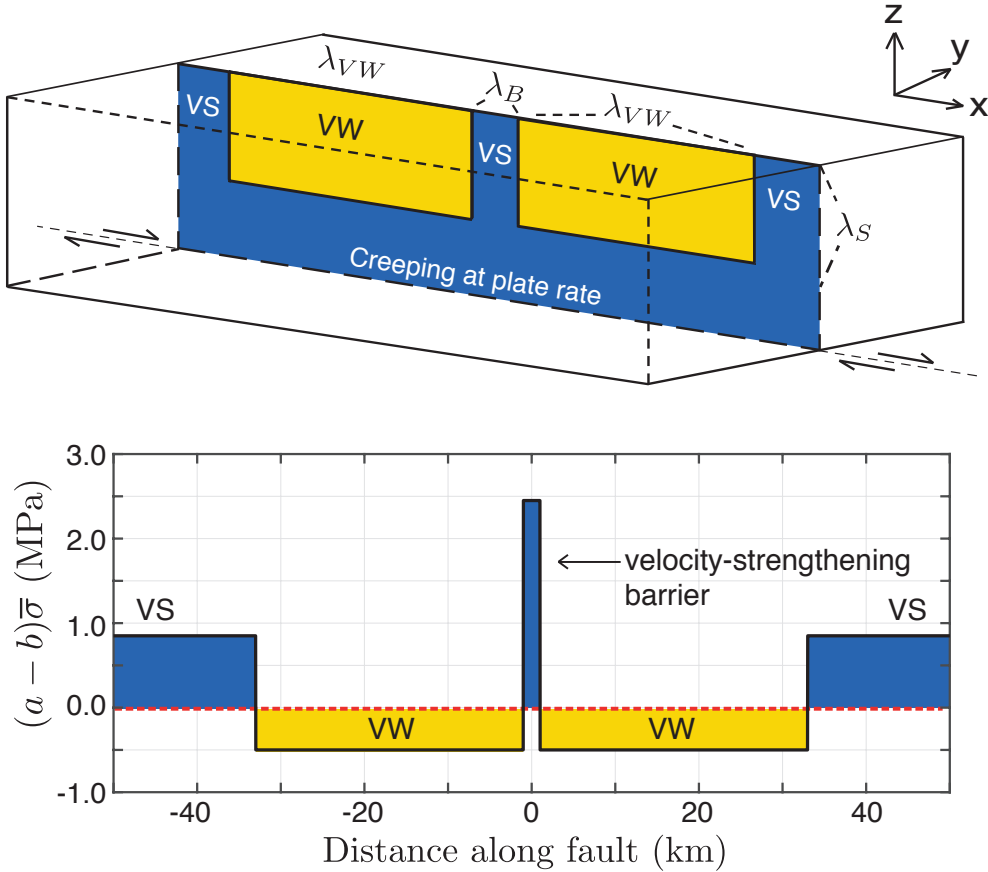
Figure 1. Schematic of a strike-slip fault with two co-planar velocity-weakening fault segments separated by a velocity-strengthening barrier. In our simulations, we use a 2D approximation of the problem with a 1D along-strike depth-averaged fault, in which the fault is assumed to be creeping at the loading plate rate $V_{\mathrm{pl}} = 10^{-9}$ m/s below the depth of $\lambda_S =$ 15 km.
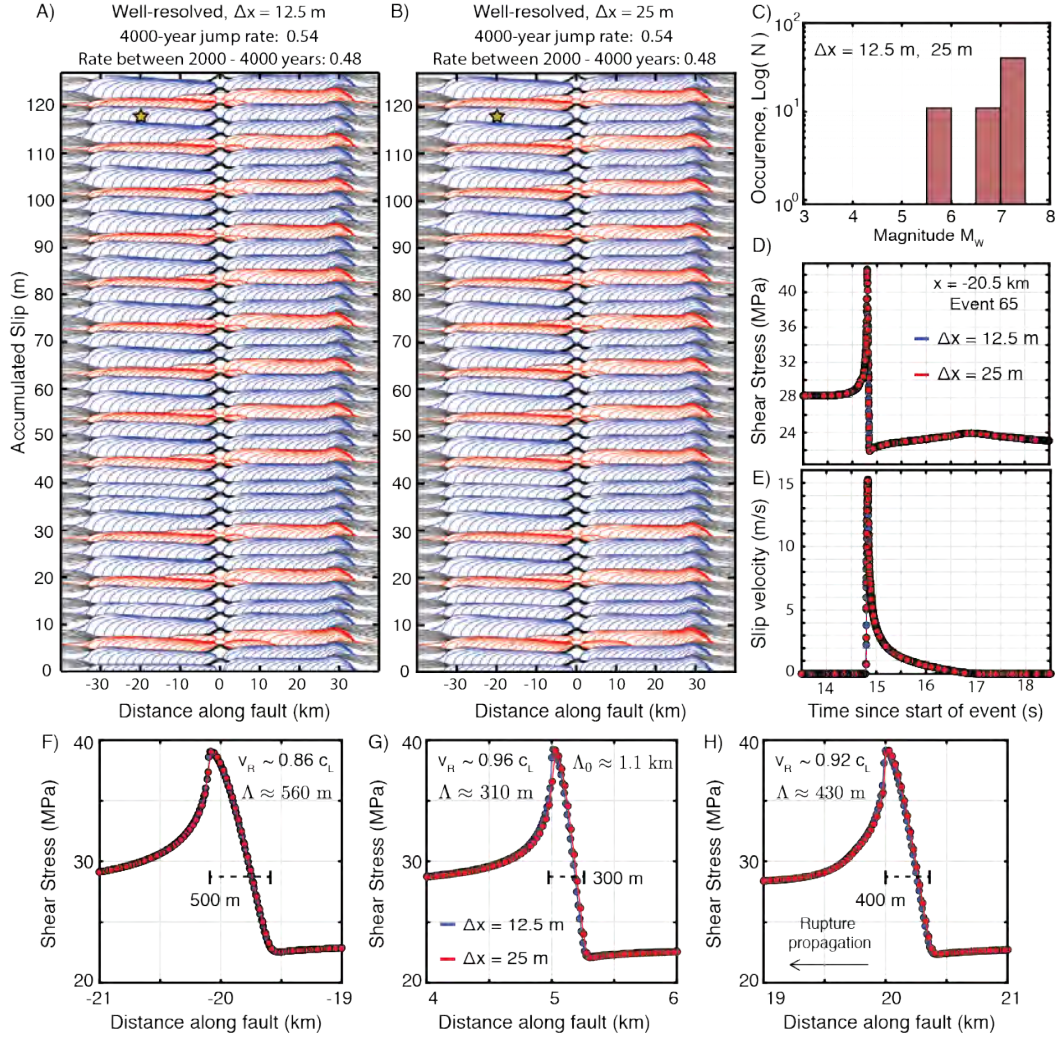
Figure 2. Interaction of two co-planar fault segments in well-resolved simulations of model M1 demonstrating convergence of simulated earthquake sequences. (A-B) History of cumulative slip over 4000 years in well-resolved fully-dynamic simulations of fault model M1 with initial conditions S1 using (A) 12.5-m and (B) 25-m cell size. Contours for seismic slip are plotted every 0.5 s, with ruptures that jump across the VS barrier colored blue. The simulated fault behavior is virtually indistinguishable between the two resolutions. (C) Frequency-magnitude histograms of events, on top of each other for the two resolutions. The well-resolved simulations produce the same relatively simple and quasi-periodic behavior. (D-E) The evolution of local shear stress and slip velocity at a point ($x = -20.5$ km, shown by star in A and B), practically indistinguishable even after over 3800 years of simulated time. (F-H) Spatial distribution of shear stress at the rupture front for three locations ($x = -20$ km, 5 km and 20km) throughout the first rupture in (A-B). While the quasi-static estimate of the cohesive zone Λ_0 is about 1.1 km, the actual size of the cohesive zone varies with the local rupture speed throughout the rupture. In these well-resolved simulations, the cohesive zone is always resolved by at least 10 cells.
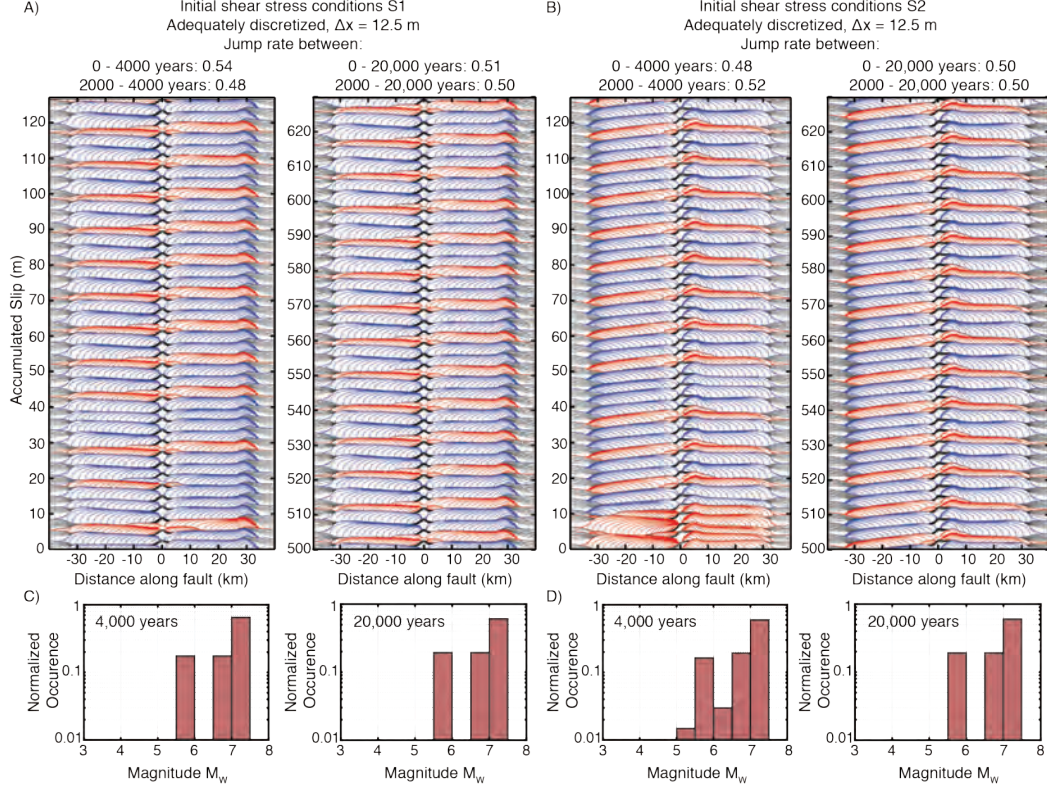
Figure 3. Convergence of well-resolved simulated earthquake sequences in model M1 for longer-term simulations and different initial conditions. (A-B) Cumulative slip over 0-4000 years and 16,000-20,000 years in two well-resolved fully-dynamic simulations of fault model M1 with two different initial conditions, S1 and S2. Contours of seismic slip are plotted every 0.5 s with ruptures that jump across the VS barrier colored blue. The quasi-periodic behavior seen in the first 4000 years in well-resolved simulations, including the rate of ruptures jumping across the VS barrier, remains generally consistent throughout longer-term simulations over 20,000 years (Right). Simulations using different initial shear stress conditions produce different initial sequences of events, however, the simulated sequences converge to the same slip behavior and have the same long-term rates of two-segment ruptures (0.50 over 2,000-20,000 years). (C-D) Normalized frequency-magnitude histograms for events from (A) and (B), respectively, over 4000 and 20,0000 years, illustrating that the population statistics in this relatively simple system is the same, apart from the initial start-up period.
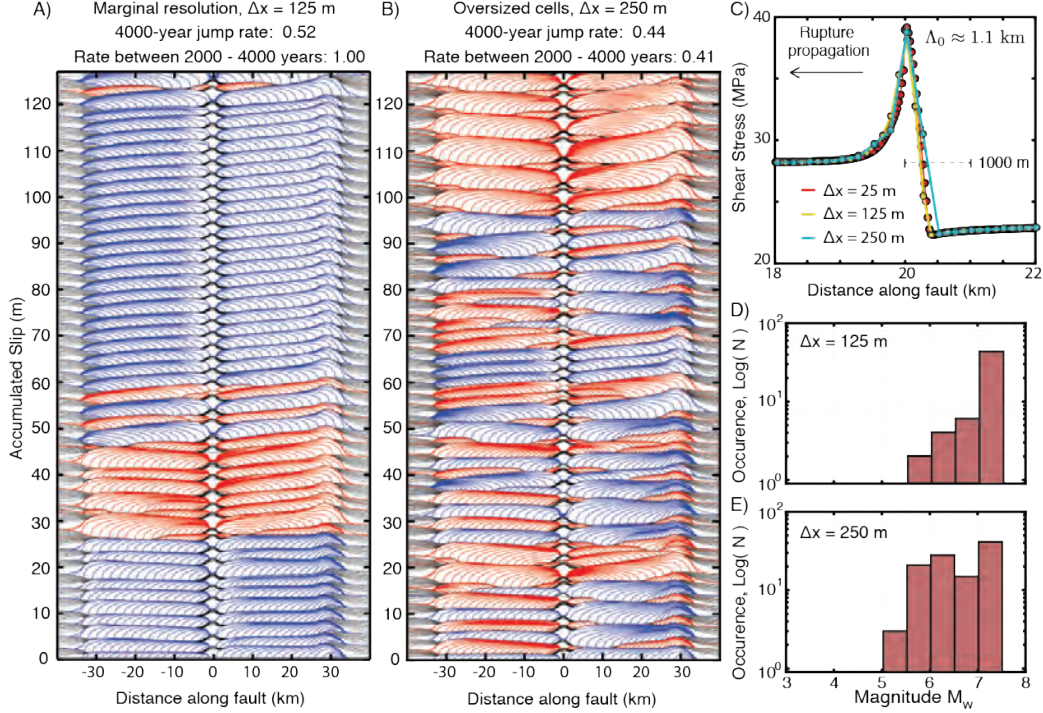
Figure 4. Less well-resolved simulations of fault model M1 exhibiting different simulated earthquake sequences and rates of two-segment ruptures. (A-B) History of cumulative slip over 4000 years in fully dynamic simulations of fault model M1 using marginal and oversized cells of (A) 125 m and (B) 250 m, respectively. Contours of seismic slip are plotted every 0.5 s, with ruptures that jump across the VS barrier colored blue. (C) Spatial distribution of shear stress around the rupture front in a well-resolved simulation ($\Delta x = 25$ m, red) and the two simulations with larger cells ($\Delta x = 125$ and 250 m). As the cell size increases, the resolution of the shear stress evolution at the rupture front decreases, although the resolution would be acceptable in simulations of single ruptures (Day et al., 2005). (D-E) Frequency-magnitude histograms for events in (A-B), respectively. The simulations with larger cells exhibit different long-term sequences of events compared to the well-resolved simulations (Fig. 2C), with increased production of small events and significantly different rates of two-segment ruptures.
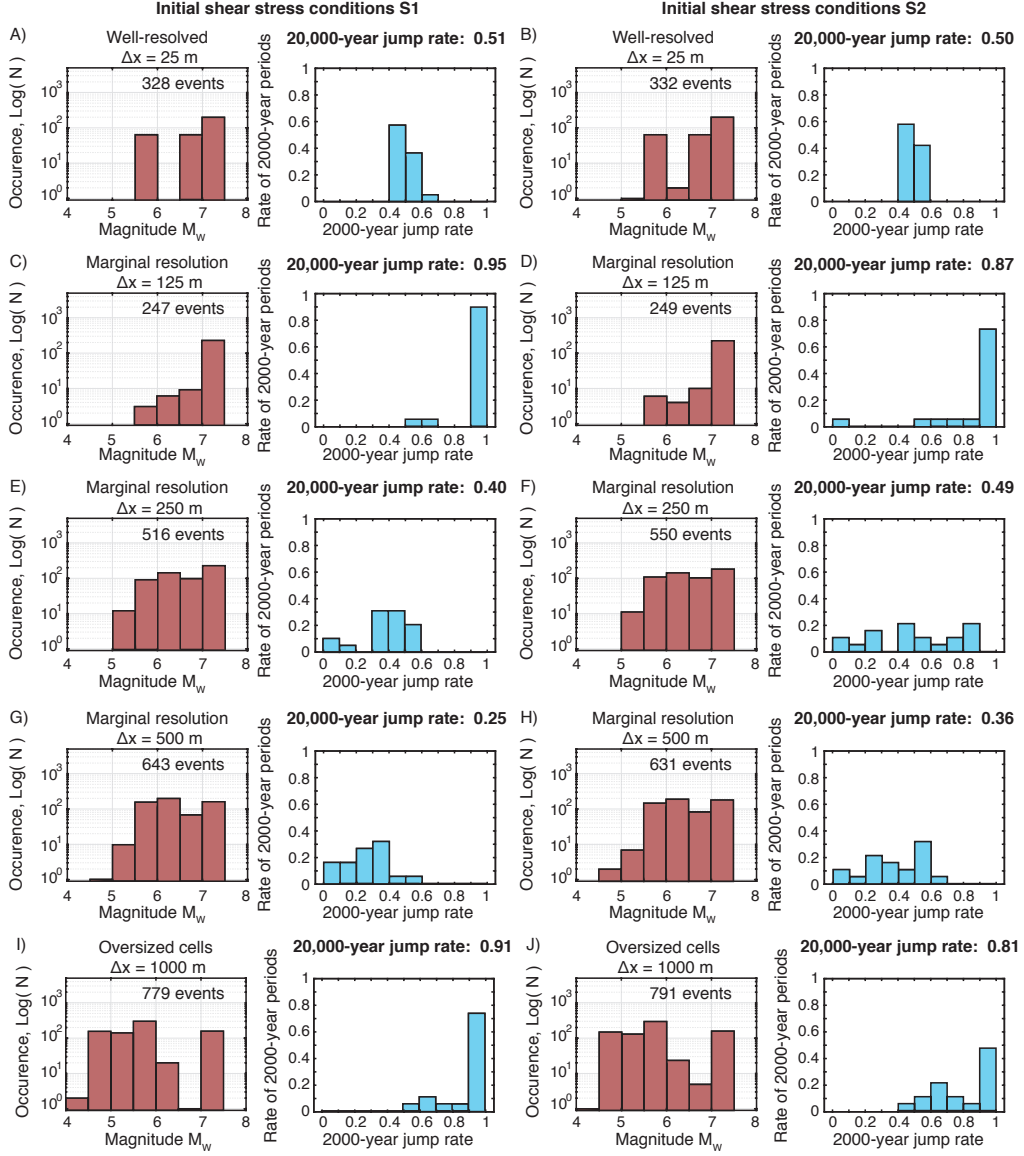
Figure 5. (A-J) Frequency-magnitude (left) and jump-rate (right) statistics for 20,000 years of simulated earthquake sequences in model M1 with different initial conditions and cell sizes. (A-B) Well-resolved simulations with different initial shear stress conditions result in comparable long-term quasi-periodic sequences, and thus comparable frequency-magnitude statistics and 2000-year jump rate statistics that are generally consistent with the 20,000-year jump rate of 0.50. (C-J) As the resolution decreases, the sequences become more complex with greater variability of event sizes and increased production of smaller events. The jump rate during different 2000-year periods also becomes more variable and can considerably differ from the true jump rate of 0.5 in the well-resolved cases.
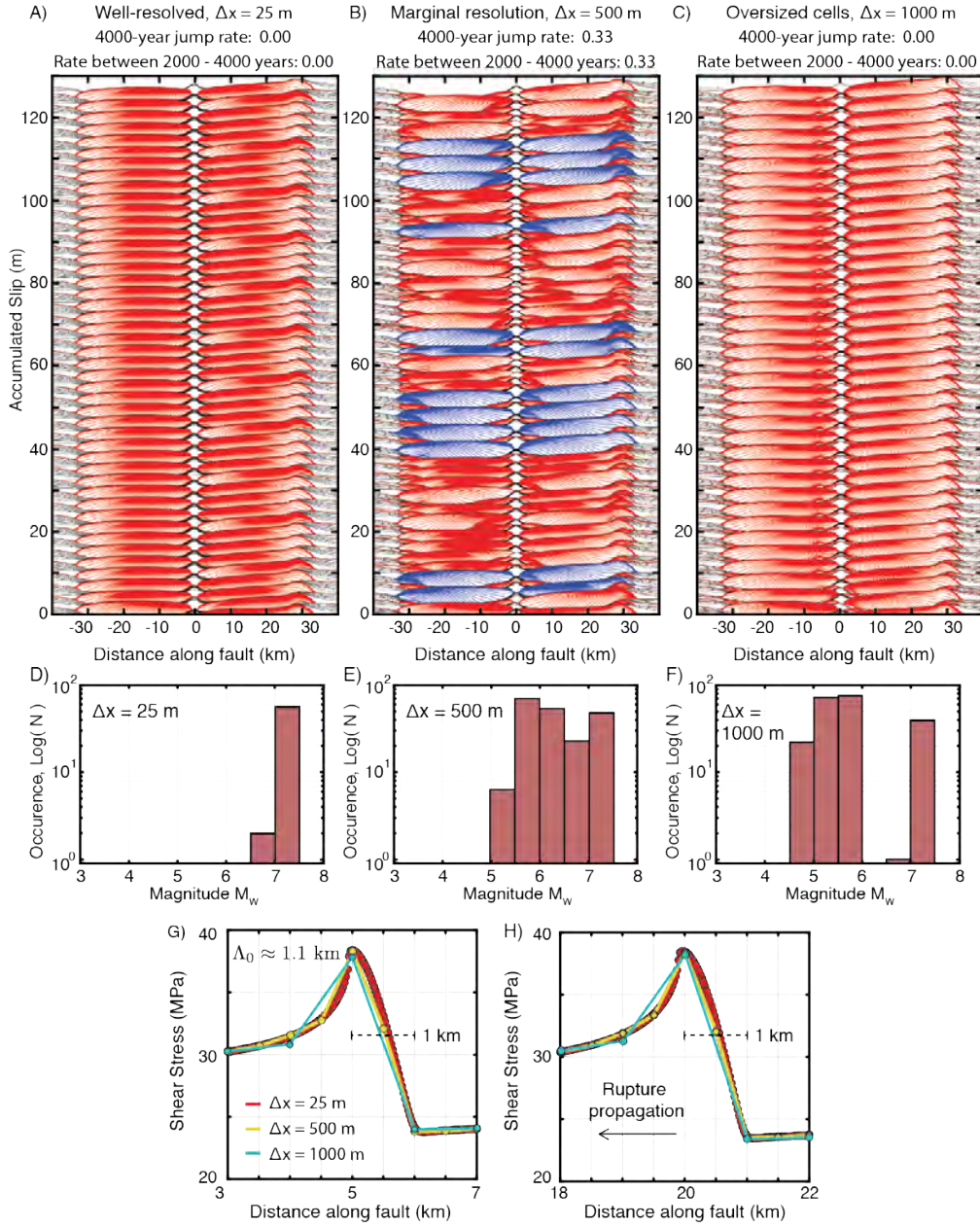
Figure 6. Interaction of two co-planar fault segments in quasi-dynamic simulations of fault model M1 with varying discretization. (A-C) History of cumulative slip over 4000 years in quasi-dynamic simulations of fault model M1 with initial conditions S1 using (A) adequate discretization, (B) marginal discretization, and (C) oversized cells. Contours of seismic slip are plotted every 0.5 s, with ruptures that jump across the VS barrier colored blue. (D-F) Frequency-magnitude histograms for events in (A-C). (G-H) Spatial distribution of shear stress illustrating the breakdown of shear resistance at the rupture front during quasi-dynamic simulations in fault model M1 with varying spatial resolution. The cohesive zone does not shrink during quasi-dynamic ruptures. A well-resolved rupture front is shown in red with a cell size of 25 m. The cohesive zone ($\Lambda_0 = 1.1$ km) is resolved by at best 1 to 2 cells for cell sizes of 500 to 1000 m.
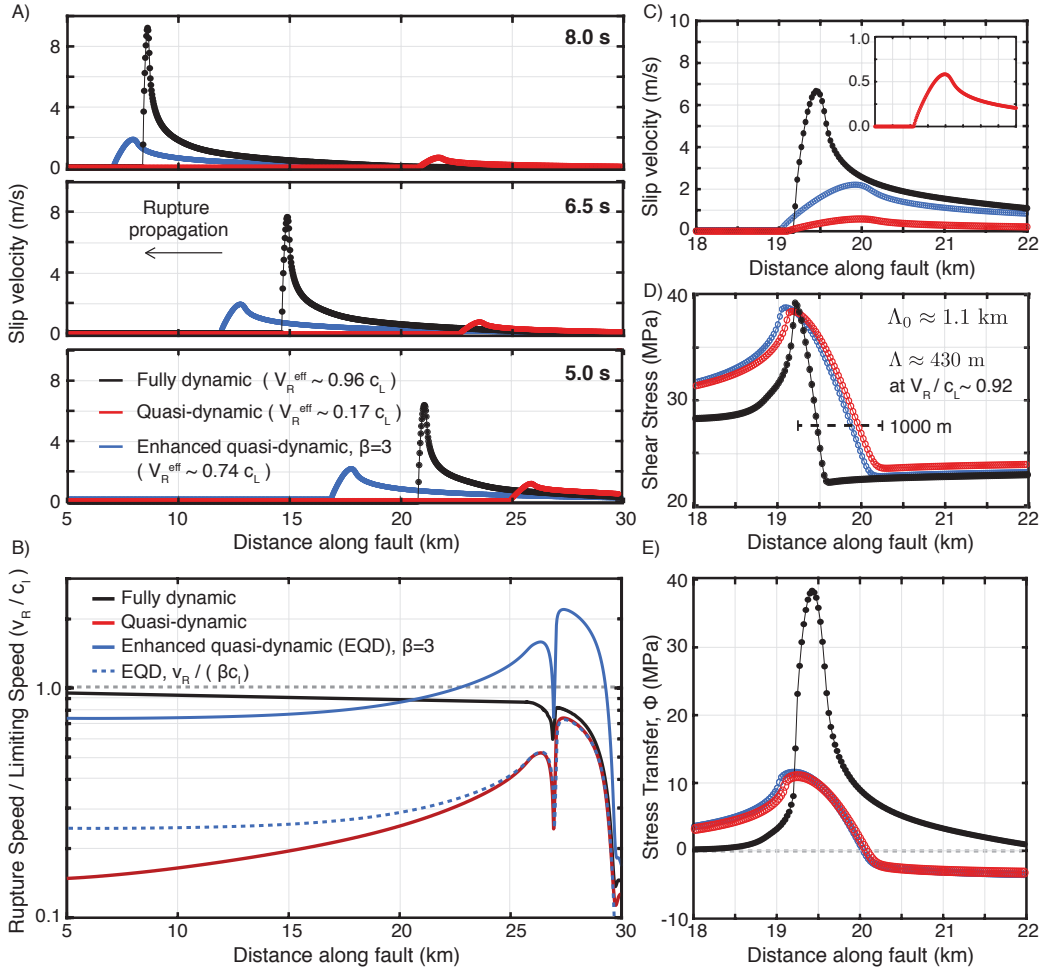
Figure 7. Comparison of local slip rate, shear stress, and rupture speed for simulations with different treatment of inertial effects. (A) Spatial distribution of slip rate at three instances of time during the first rupture with the same initial conditions in fully dynamic (black), quasi-dynamic (red) and enhanced quasi-dynamic (blue) simulations of fault model M1. (B) The fully dynamic rupture accelerates to a rupture speed close to the limiting wave speed of $c_L \approx 4.4$ km/s throughout the rupture, whereas the quasi-dynamic ruptures maintain lower effective rupture speeds. Decreasing the radiation damping term for quasi-dynamic ruptures increases the slip rate and rupture speed, but does not truly mimic the acceleration of the fully dynamic rupture. (C-D) A closer look at the spatial distribution of (C) slip velocity and (D) shear stress at a given time highlights how full consideration of inertial effects leads to much higher slip velocities and a more localized stress concentration at the rupture front, which facilitates rupture propagation. Enhancing the quasi-dynamic ruptures with lower radiation damping increases the slip rate but maintains the same quasi-static spatial pattern of stress at the rupture front. (E) The corresponding values of the stress transfer functional near the rupture front. The radiation damping approximation of the inertial effects results in dramatically reduced stress transfer along the fault. The larger total stress transfer in the fully dynamic simulations is balanced by higher slip rates, as shown in (C).
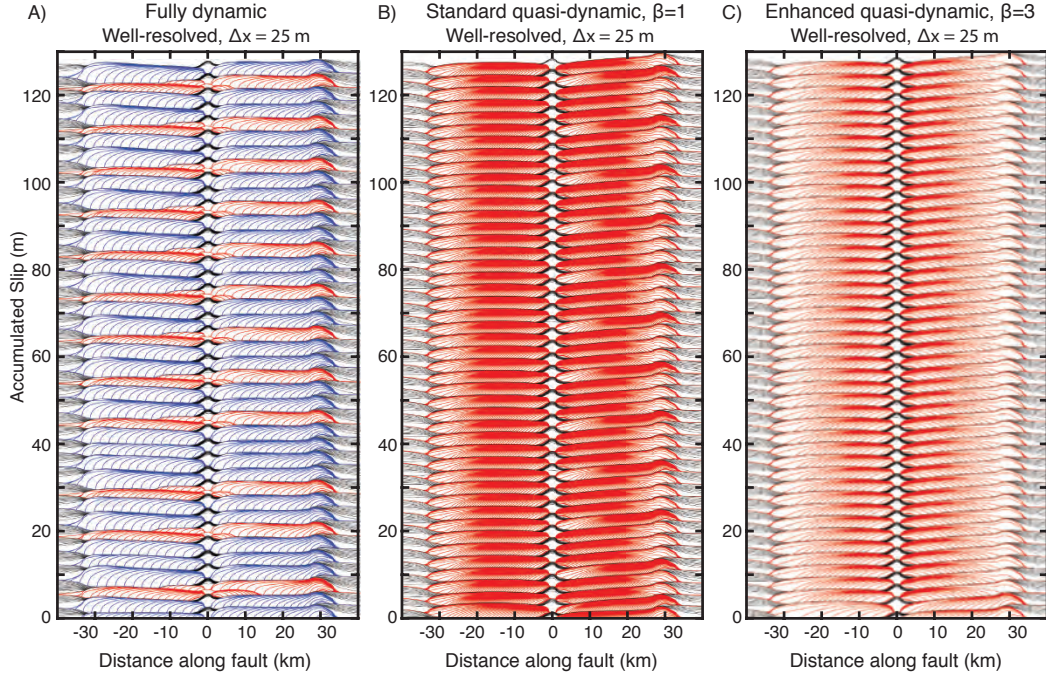
Figure 8. Different long-term interaction of co-planar fault segments in simulations with different treatment of inertial effects. (A-C) History of cumulative slip over 4000 years in well-resolved (A) fully dynamic, (B) standard quasi-dynamic ($\beta = 1$) and (C) enhanced quasi-dynamic ($\beta = 3$) simulations of fault model M1 with initial conditions S1. Contours of seismic slip are plotted every 0.5 s. The increased spacing between contours for the enhanced quasi-dynamic ruptures in (C) illustrate the higher effective rupture speeds that are more comparable to those of the fully dynamic ruptures in (A). Despite the higher rupture speeds and larger slip rates (Figure 7), the long-term slip behavior for both quasi-dynamic simulations is qualitatively comparable, with no ruptures jumping across the VS barrier.
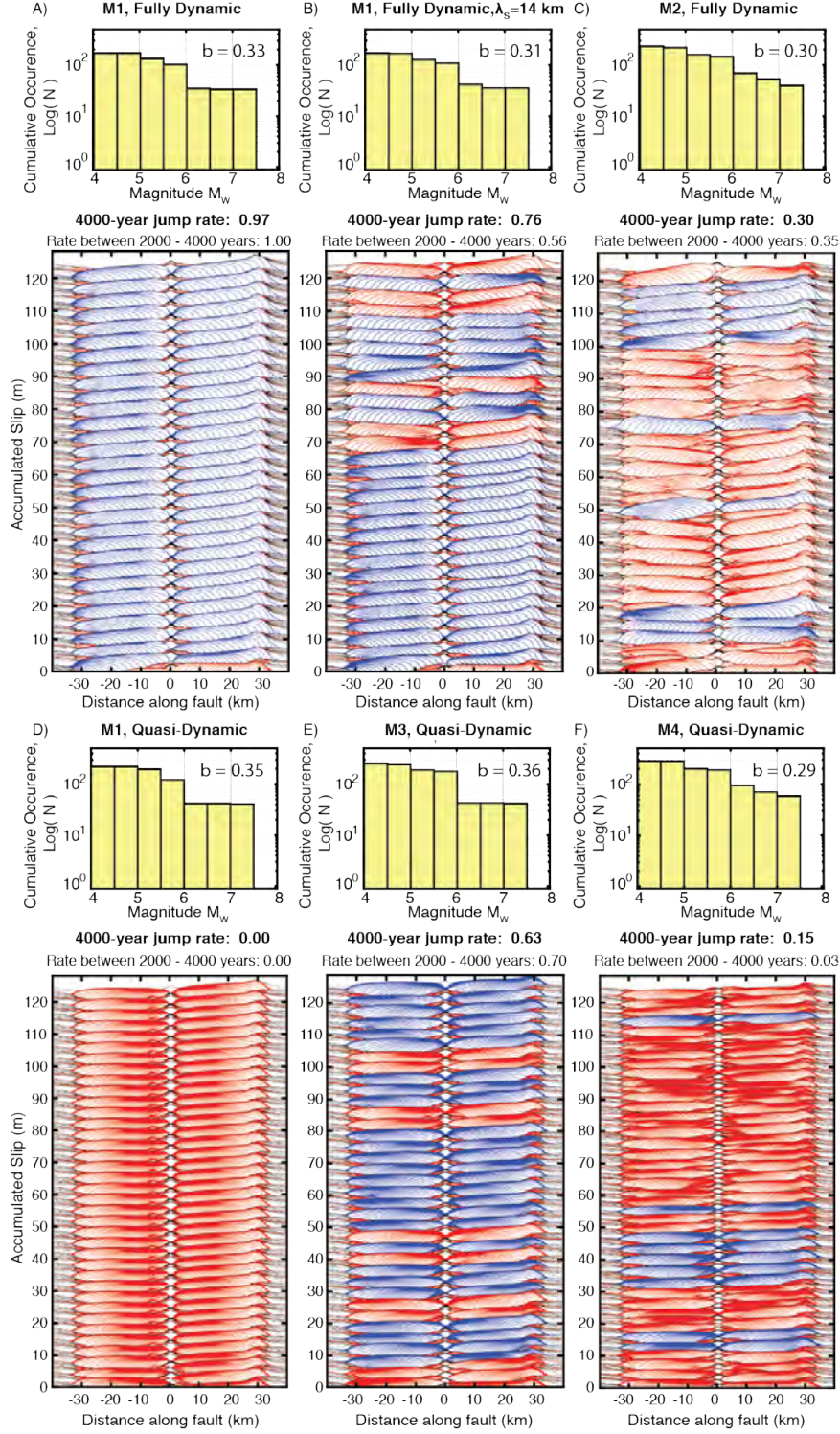
Figure 9. Models with comparable frequency-magnitude statistics and static stress drops but very different rate of two-segment ruptures. (A-F) Cumulative frequency-magnitude histograms (top) and history of cumulative slip (bottom) over 4000 years in (A-C) fully dynamic and (D-F) quasi-dynamic SEAS simulations. The simulations assume different physical conditions described in the text. All six simulations produce comparable average static stress drops (Supplementary Figure S3) and comparable population statistics with a b-value around 0.33. However, the rate of two-segment ruptures varies from 0 to 1.
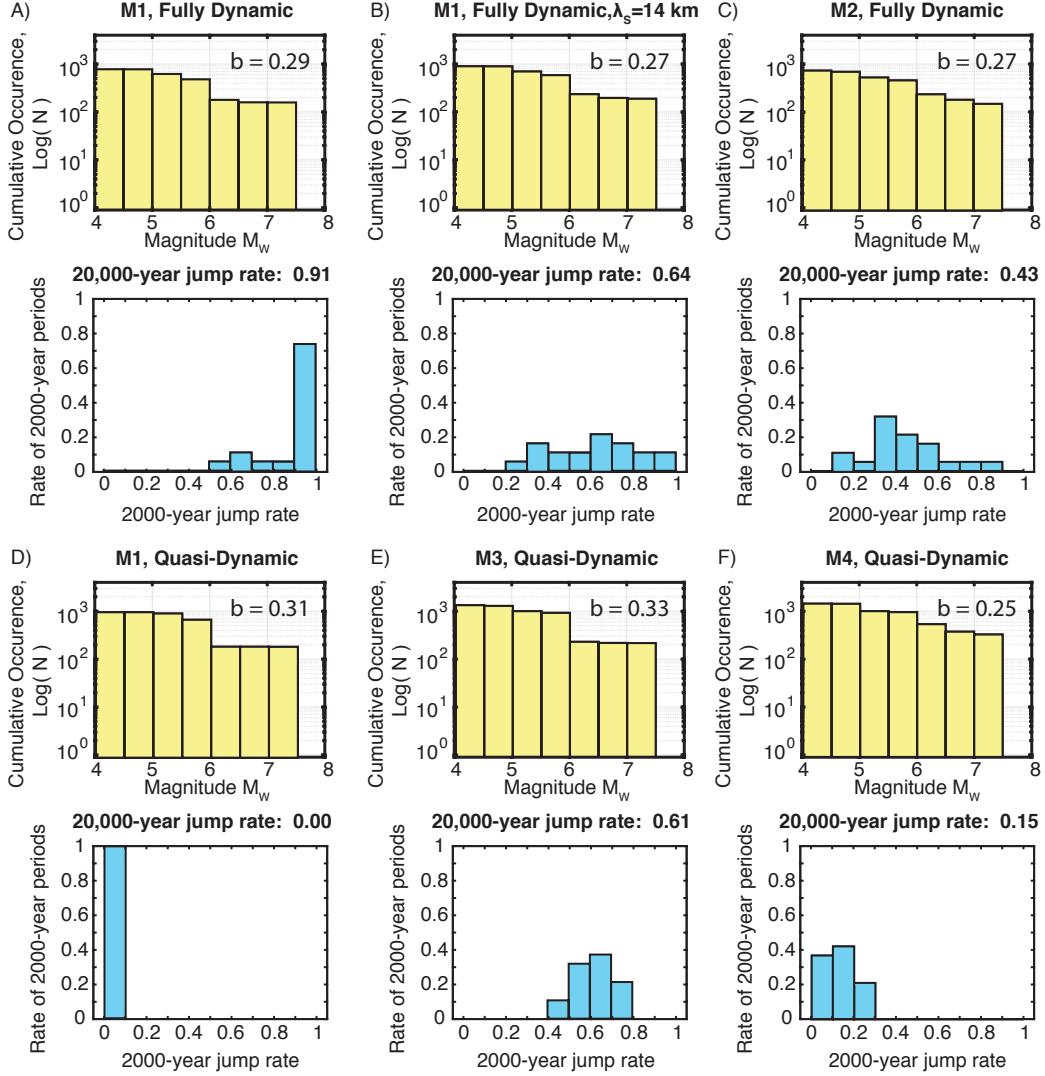
Figure 10. Variability of jump rates in models with comparable frequency-magnitude statistics and static stress drops. (A-F) Cumulative frequency-magnitude histograms (Top) and normalized 2000-year jump rate histograms (Bottom) over 20,000 years in (A-C) fully dynamic and (D-F) quasi-dynamic SEAS simulations, as shown in Figure 9. The six simulations have comparable frequency-magnitude statistics but the 20,000-year rate of two-segment ruptures varies from 0 to 0.91. The distribution of 2000-year jump rates is also highly variable among the six simulations.
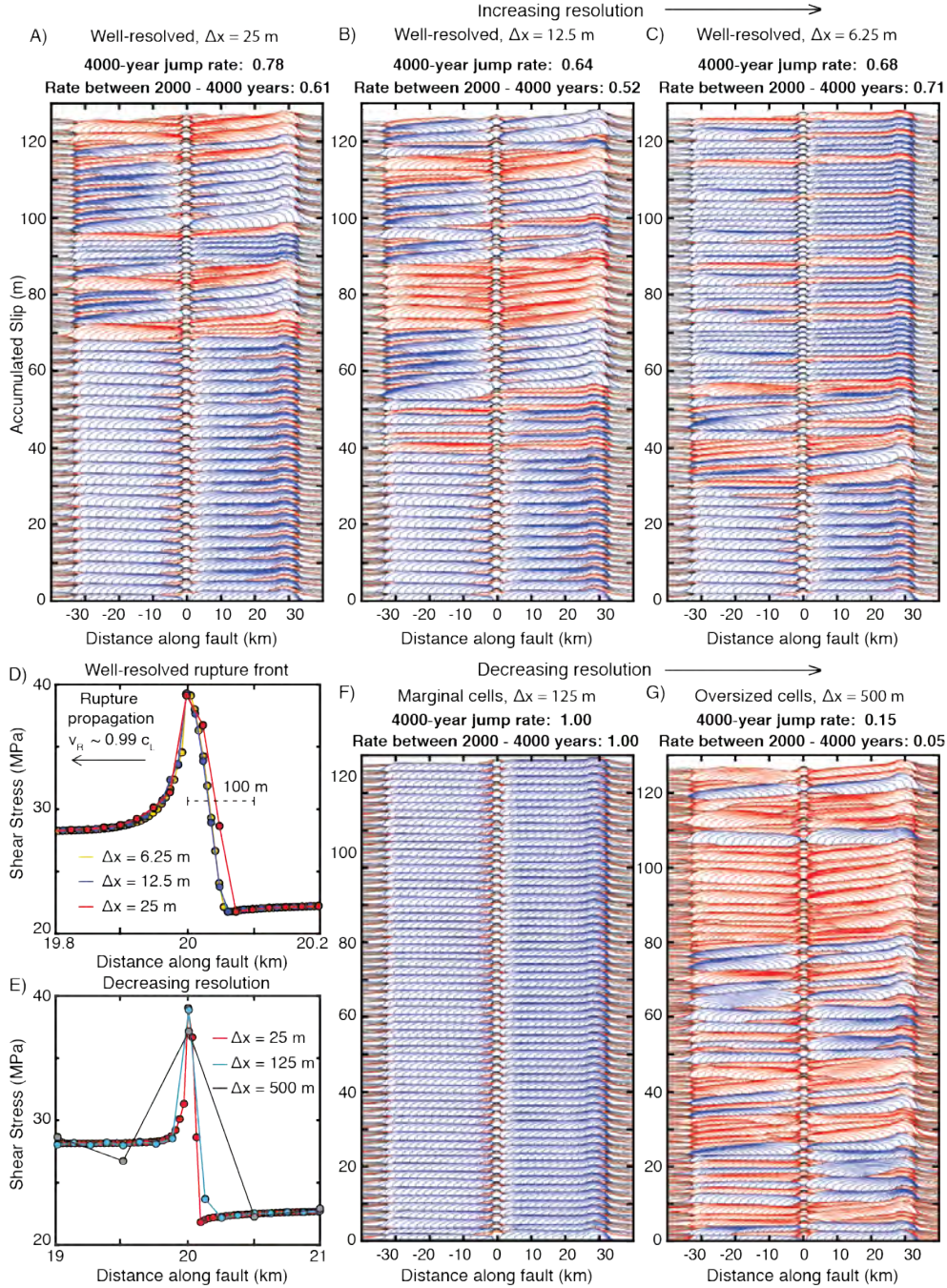
Figure 11. Sequences of earthquakes and rates of two-segment ruptures over 4000 years in fully dynamic simulations with different resolution of fault model M5 with higher instability ratio. Seismic slip is contoured every 0.5 s with ruptures jumping across the VS barrier colored blue. (A-C) Slip history for increasingly better-discretized simulations. While the initial 1000 years of simulated behavior appear well resolved and comparable, longer-term simulations begin to diverge due to the compounded effects of small numerical differences, leading to similar but inconsistent jump rates across the barrier. (D-E) The spatial distribution of shear stress at the rupture front. For well-resolved simulations (D), the cohesive zone is resolved by several cells, but is resolved by less than even one cell for poorly-resolved simulations (E). (F-G) Simulations with decreasing numerical resolution can exhibit additional artificial complexity and substantially different long-term fault behavior, including different rates of two-segment ruptures.
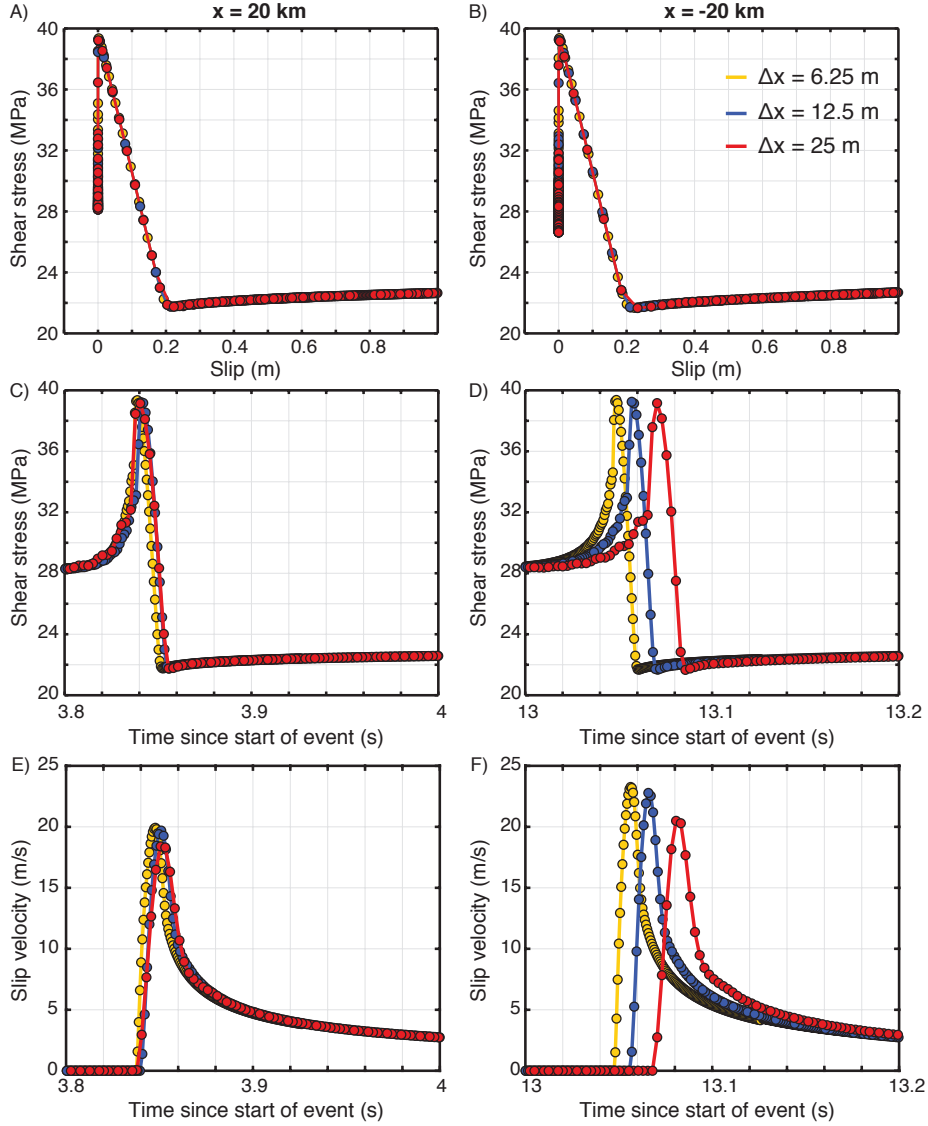
Figure 12. Excellent resolution of local shear stress and slip rate for the first rupture of well-resolved fully dynamic simulations of model M5 shown in Figure 11. The evolution of local shear stress with slip at (A) $x = 20$ km and (B) $x = -20$ km is virtually identical. Evolution of (C-D) shear stress and (E-F) slip rate with time for the same points. The rupture nucleates near $x = 30$ km. Early in the rupture (A, C & E), the local behavior is comparable among the well-resolved simulations. Near the end of the first rupture (D & F), the simulations begin to deviate very slightly in their local behavior, consistent with the results of Day et al. (2005). While the simulated behavior in the first rupture is very similar, these small differences, resulting from different numerical approximations, compound over many sequences and eventually lead to diverging behavior, as seen in Figure 11.
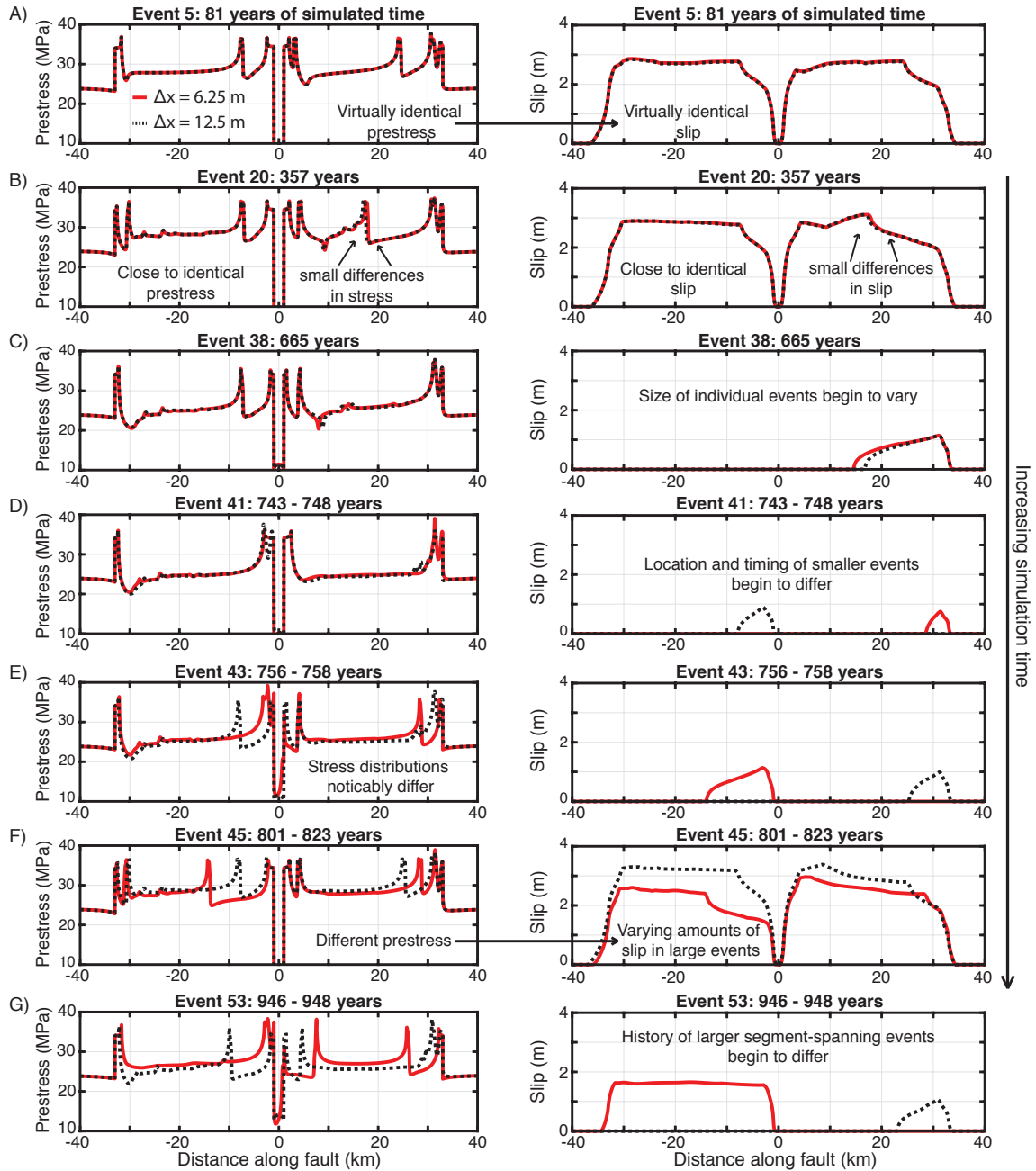
Figure 13. Compounded effects of minor numerical differences in well-resolved simulations of model M5 result in diverging long-term earthquake sequences. Comparison of the prestress before rupture (left) and resulting slip distributions (right) for several events over the first 1000 years of simulated time in two fully dynamic simulations of fault model M5 using cell sizes of 6.25 m (red) and 12.5 m (black). (A & B) The evolution of shear stress and accumulation of slip during the first few hundred years of simulated time are virtually identical. (C-E) Eventually, small differences in shear stress before events build up due to different numerical approximations, resulting in small differences in slip and rupture length for individual events, as well as the location and timing for the nucleation of smaller events. (F & G) The differences in shear stress accumulate over sequences of events, resulting in noticeable variations of slip in larger events after 800 years of simulated time and, eventually, different histories of large segment-spanning events between the two well-resolved simulations, as shown in Figure 11.
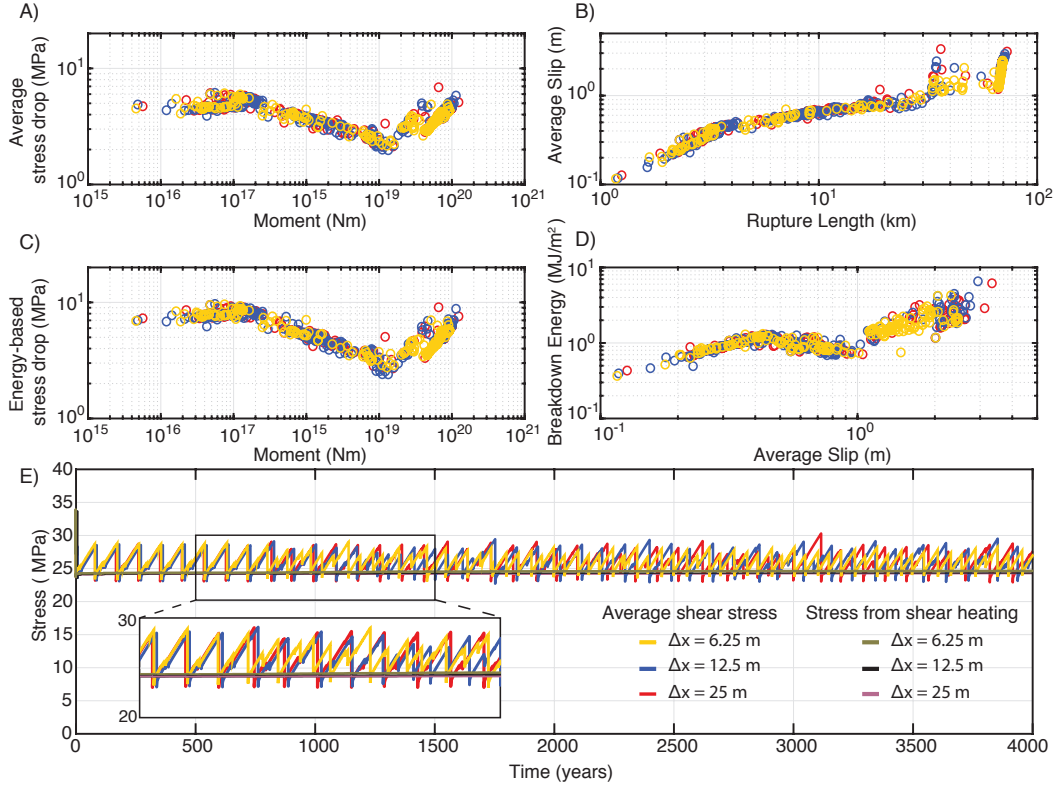
Figure 14. Averaged source properties and fault behavior that are generally consistent among well-resolved fully dynamic simulations of fault model M5, despite lack of convergence of slip with finer resolution. (A) Spatially-averaged stress drop versus moment. (B) Average slip versus rupture length. (C) Energy-based average stress drop versus moment. (D) Average breakdown energy versus average slip. (E) Evolution of average shear stress and the shear stress associated with shear heating over 4000 years of simulated sequences of earthquakes. It is apparent that the timing and degree of slip of individual events in the sequences of earthquakes differ. However the general characteristics of the overall average stress evolution, in terms of the maximum and minimum stresses and the average stress drops, are comparable, resulting in virtually indistinguishable shear heating stresses.
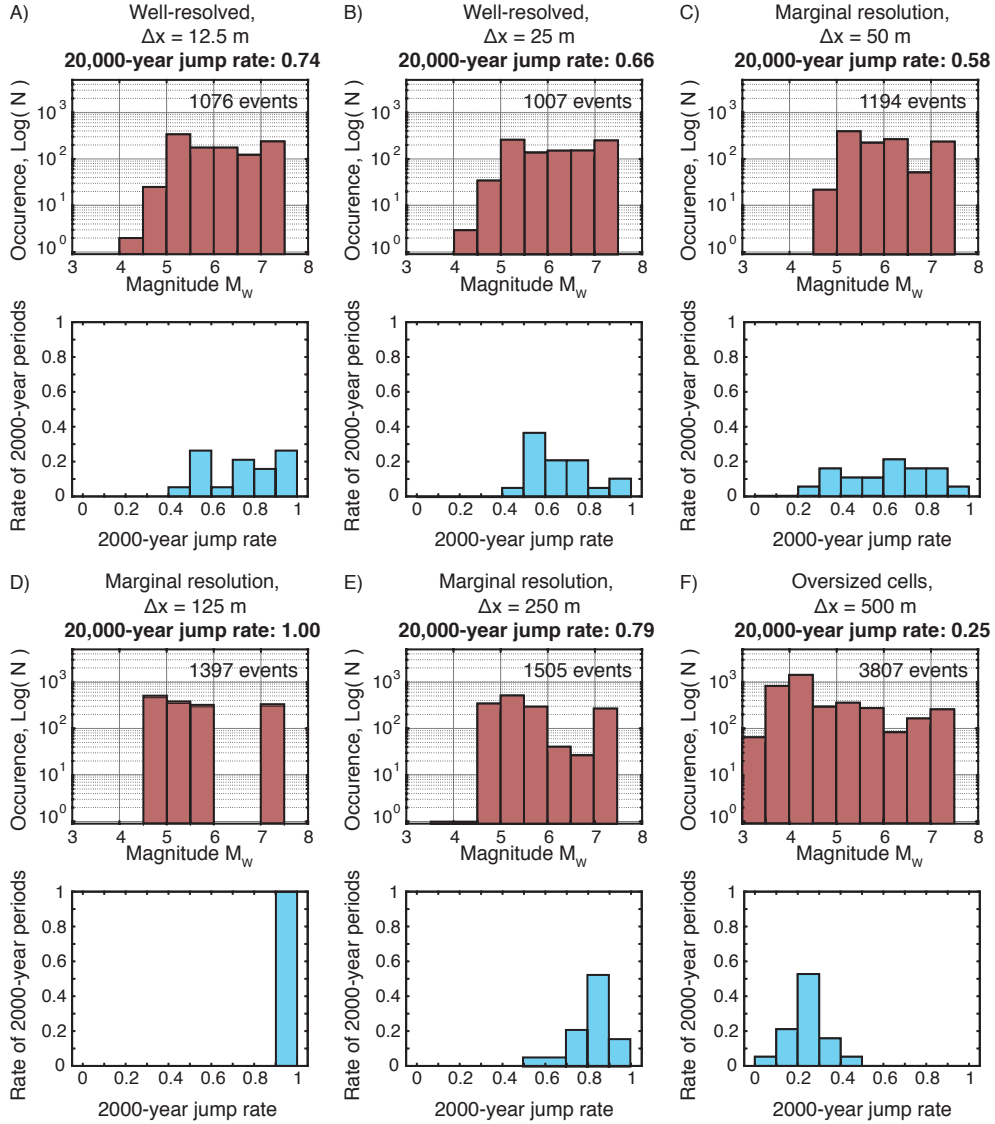
Figure 15. Different frequency-magnitude and jump rate statistics for 20,000 years of sequences of earthquakes in fully dynamic simulations of fault model M5 with varying cell sizes. (A-F) Frequency-magnitude histograms (Top) and normalized 2000-year jump rate histograms (Bottom) for 20,000 years of simulated SEAS. (A-B) Even well-resolved simulations exhibit mild differences in long-term event statistics, though the frequency-magnitude histograms are similar. The 2000-year jump rate histograms are different but comparable for well-resolved simulations, with the 20,000-year jump rate varying by approximately 15% among the three simulations. (C-F) Simulations with marginal or inadequate resolution have enhanced production of smaller events, as small groups of cells nucleate into ruptures but fail to propagate substantially due to poorly resolved stress concentration at the rupture front. The 20,000-year jump rates and 2000-year jump rate distributions substantially vary for simulations using oversized cells compared to the well-resolved simulations.
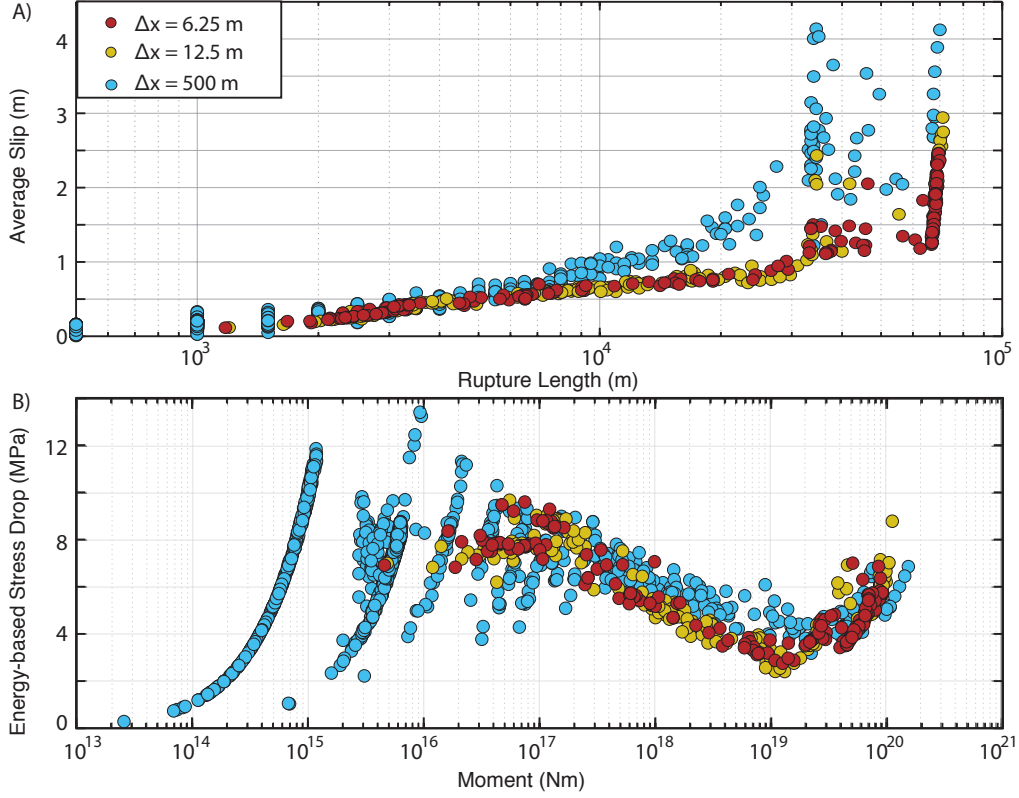
Figure 16. Scaling of average slip and stress drop with rupture size for numerically-discrete versus well-resolved ruptures in fault model M5. (A-B) Despite different long-term sequences of events, two well-resolved simulations of fault model M5, with cell sizes $\Delta x = 6.25$ m and $\Delta x = 12.5$ m, have similar scaling of average slip and static stress drop with rupture size. Simulations using oversized cells produce small numerically-discrete ruptures consisting of only a few cells that fail to propagate due to the poorly resolved stress concentration of the shear stress at the (diffuse) rupture front. This causes large ruptures to occur in poorly-resolved simulations for higher values of shear stress, resulting in large ruptures having greater average slip than in well-resolved simulations (A). The small numerically-discrete ruptures produce variable amounts of slip, despite being restricted to the same rupture size of only 1 to several cells (A), leading to large, upward-sweeping trends in average stress drop with moment, which are purely numerical (B).
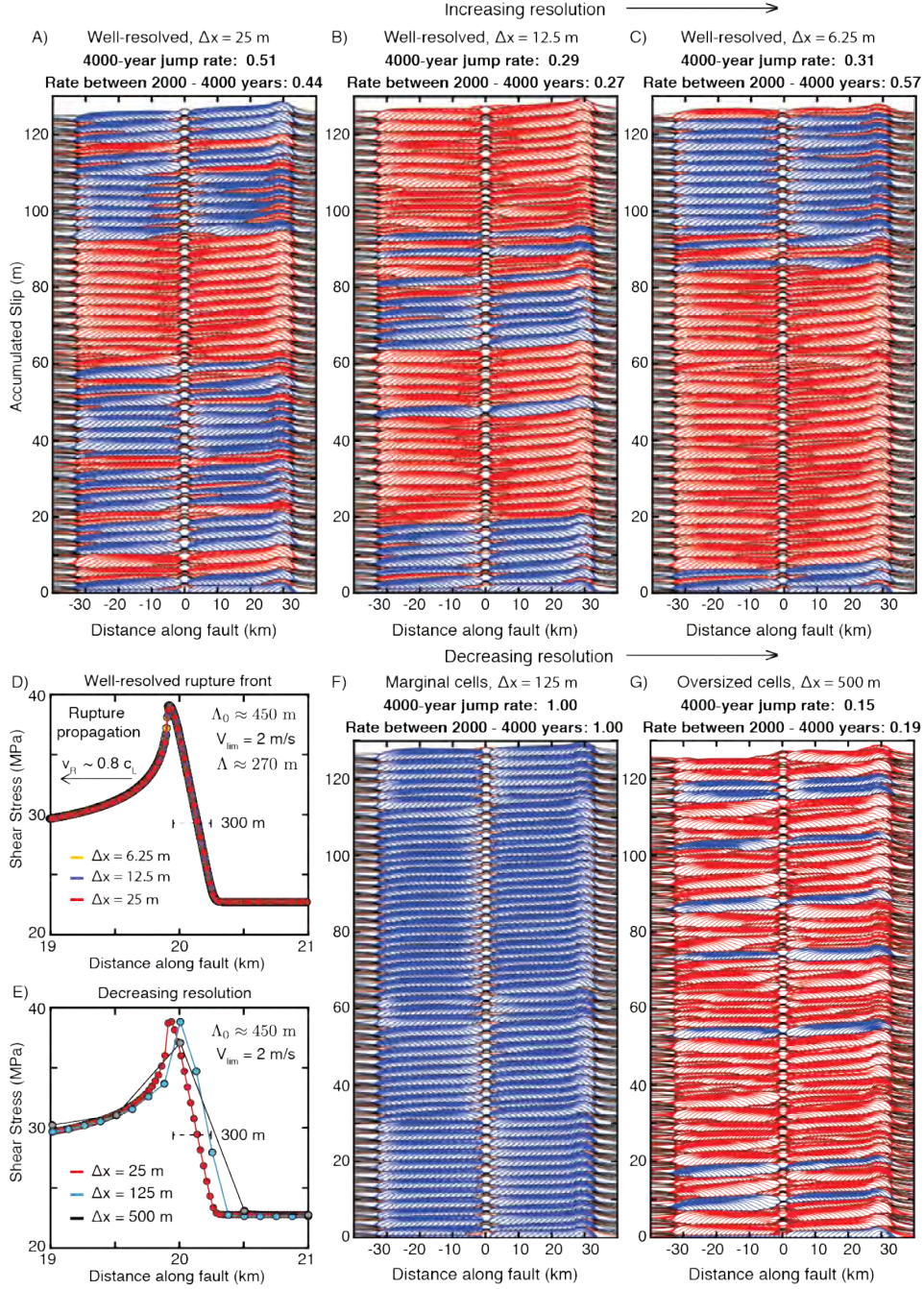
Figure 17. Sequences of earthquakes and rate of two-segment ruptures over 4000 years in fully dynamic simulations with different resolution of fault model M5 and an approximation of off-fault plasticity. The rupture speed reduces to 0.8 c_L due to the approximation using a velocity limit of $V_{\lim} = 2$ m/s. Seismic slip is contoured every 0.5 s with ruptures jumping across the VS barrier colored blue. (A-C) Slip history for increasingly well-resolved simulations. The initial few sequences of events appear comparable among well-resolved simulations, however the sequences begin to differ due to the compounded effects of small numerical differences. (D-E) The cohesive zone shrinks by only about a factor of two for rupture speeds below 0.8 c_L, so the rupture front is very well-resolved. (F-G) Simulations with decreasing numerical resolution exhibit additional artificial complexity and substantially different long-term fault behavior, including rates of two-segment ruptures.
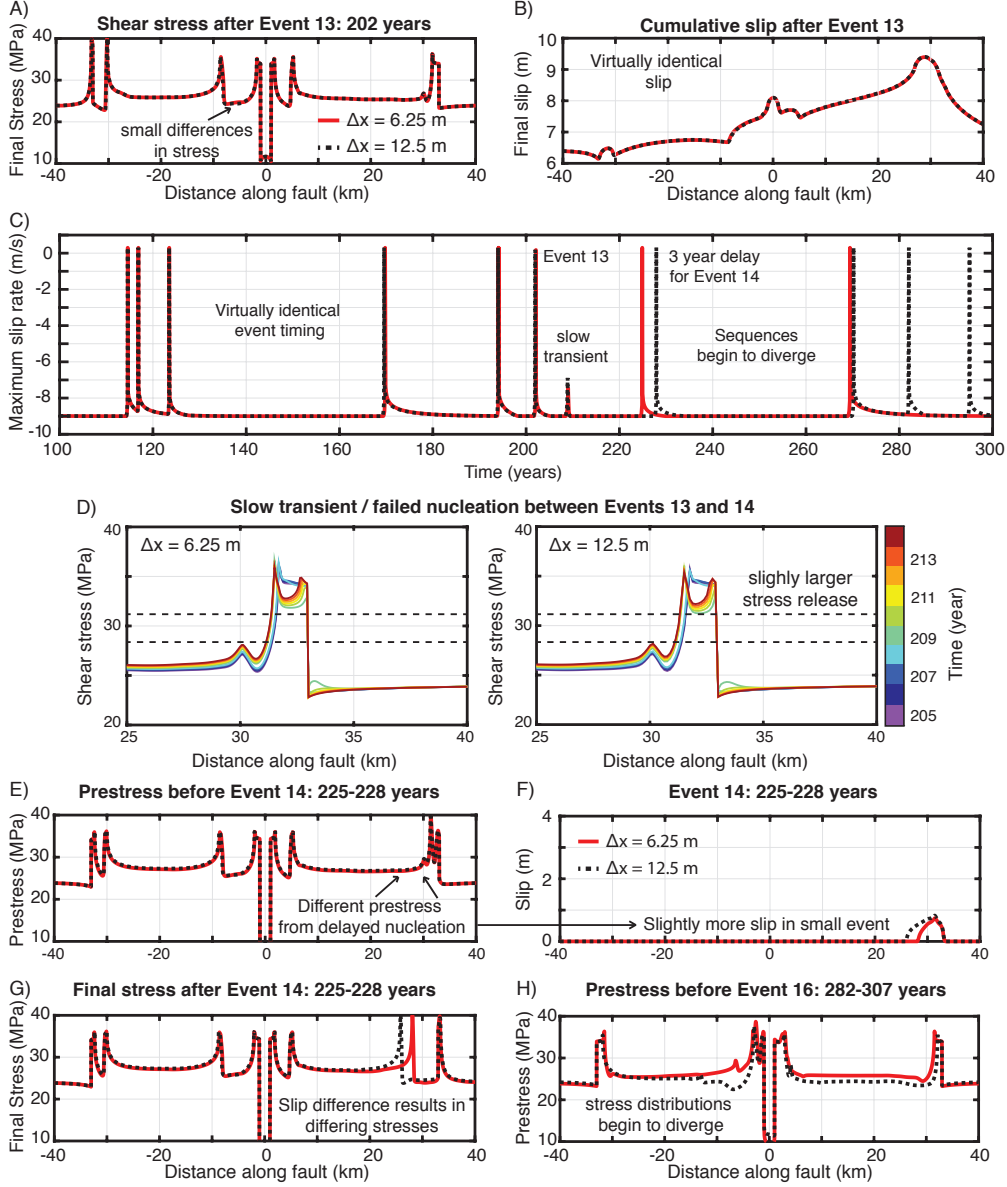
Figure 18. Simulations with diverging long-term sequences of earthquakes after small differences in a slow-slip transient. (A-B) Virtually indistinguishable spatial distribution of shear stress and slip after the 13th event in fully dynamic simulations of fault model M5 with the effects of off-fault dissipation approximated using a velocity limit of $V_{\text{lim}} = 2$ m/s, with cell sizes of $\Delta x = 6.25$ (red) and $\Delta x = 12.5$ (black dashed). (C) Evolution of the maximum slip rate between 100 to 300 years of simulated time. Before event 13 the timing of slip events is nearly identical, however after a slow-slip transient following event 13, around $t = 210$ years, the timing of slip events begins to diverge. (D) The resolved shear stress changes due to the slow-slip transient within the nucleation region of event 14 mildly differs between the two simulations of different cell size, resulting in a slightly higher stress release for the simulation with cell size $\Delta x = 12.5$ m. (E-F) Following the slow-slip transient, there is a 3-year difference between the nucleation of event 14, leading to slightly higher prestress before the initiation of the rupture, and hence slightly different resulting slip distributions. (G-H) The different rupture sizes and amount of slip in event 14 results in differing final stress distributions. The timing of subsequent events becomes more disparate between the two simulations and the shear stress distributions and sequences of events begin to differ more substantially (Figure 17).
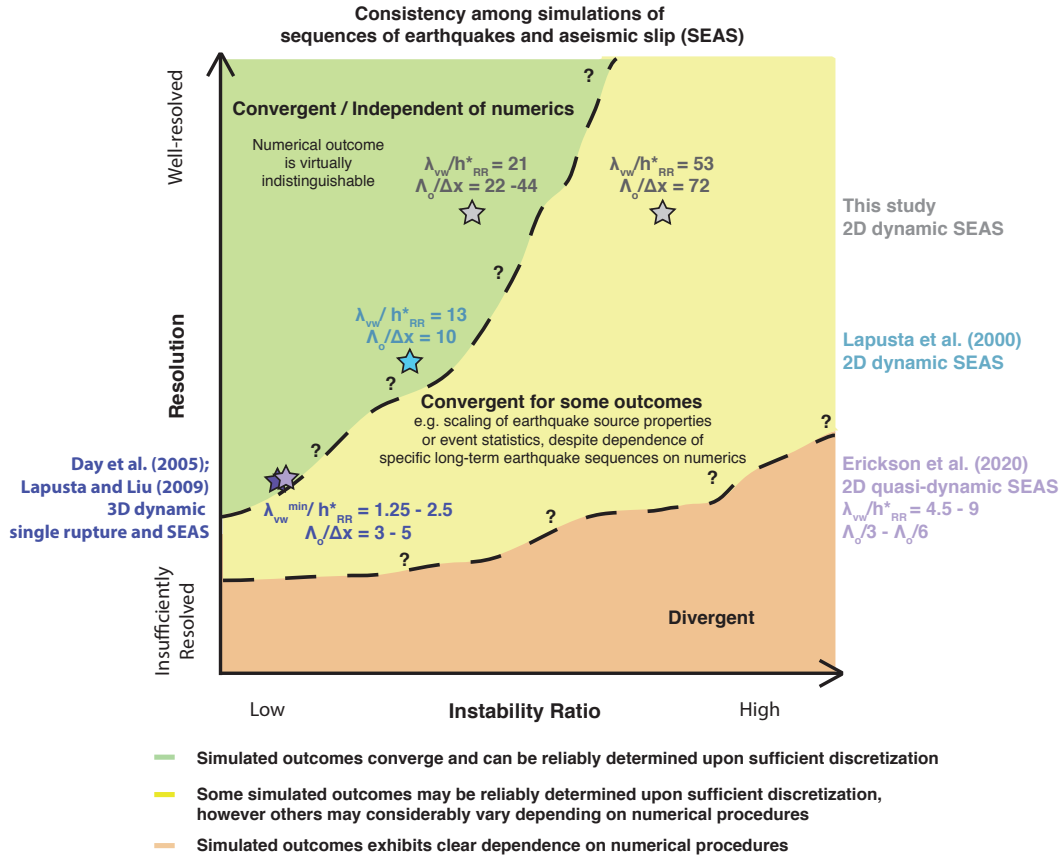
Figure 19. Conceptual diagram illustrating potentially convergent versus divergent numerical behavior depending on resolution and model complexity, parameterized by the instability ratio as an example. Well-resolved fault models with low enough instability ratio may potentially be numerically deterministic where adequate discretization results in virtually indistinguishable numerical outcomes. Fault models with higher instability ratio may either have more stringent requirements for numerical discretization in order to achieve long-term convergence, or such convergence may be impossible; either way, achieving numerical convergence in simulations of sufficiently complex fault models, such as with higher instability ratios, would be impractical. In such cases, it may still be possible to achieve statistical consistency among some outcomes within well-resolved simulations, though other properties of the system may be highly sensitive to numerical precision and considerably vary depending on the numerical procedures.
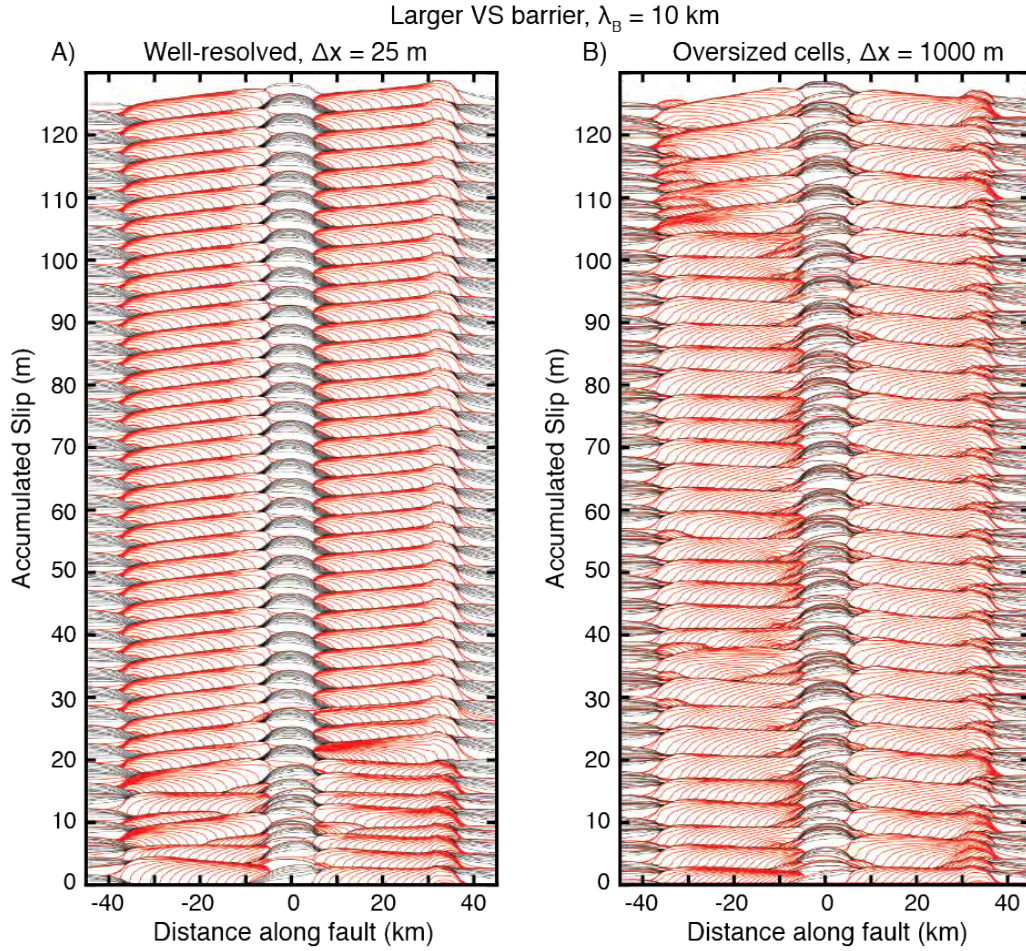
Figure 20. Consistent isolation of ruptures on fault segments separated by a larger velocity-strengthening barrier in simulations with adequate discretization and oversized cells. History of cumulative slip over 4000 years in two fully dynamic simulations of fault model M1 that utilize (A) cells that adequately resolve the cohesive zone ($\Delta x = 25$ m) and (B) oversized cells ($\Delta x = 1000$ m). Seismic slip is contoured every 0.5 s. The VS barrier is increased in width to 10 km such that ruptures are isolated to individual fault segments in both simulations.

References

Allison, K. L., & Dunham, E. M. (2018). Earthquake cycle simulations with rate-and-state friction and power-law viscoelasticity. *Tectonophysics*, *733*, 232 - 256. doi: 10.1016/j.tecto.2017.10.021

Allmann, B. P., & Shearer, P. M. (2009). Global variations of stress drop for moderate to large earthquakes. *Journal of Geophysical Research: Solid Earth*, *114*(B1). doi: 10.1029/2008JB005821

Ando, R., & Kaneko, Y. (2018). Dynamic rupture simulation reproduces spontaneous multifault rupture and arrest during the 2016 Mw 7.9 Kaikoura earthquake. *Geophysical Research Letters*, *45*(23), 12,875-12,883. doi: 10.1029/2018GL080550

Andrews, D. J. (2004, 06). Rupture Models with Dynamically Determined Breakdown Displacement. *Bulletin of the Seismological Society of America*, *94*(3), 769-775. doi: 10.1785/0120030142

Andrews, D. J. (2005). Rupture dynamics with energy loss outside the slip zone. *Journal of Geophysical Research*, *110*. doi: 10.1029/2004JB003191

Bak, P., & Tang, C. (1989). Earthquakes as a self-organized critical phenomenon.

manuscript submitted to *JGR-Solid Earth*

Journal of Geophysical Research: Solid Earth, *94*(B11), 15635-15637.   doi: 10 .1029/JB094iB11p15635

Barall, M., & Harris, R. A. (2014, 11). Metrics for Comparing Dynamic Earthquake Rupture Simulations. *Seismological Research Letters*, *86*(1), 223-235. doi: 10 .1785/0220140122

Barbot, S., Lapusta, N., & Avouac, J.-P. (2012). Under the hood of the earthquake machine: Toward predictive modeling of the seismic cycle. *Science*, *336*(6082), 707-710.

Ben-Zion, Y., & Rice, J. R. (1995). Slip patterns and earthquake populations along different classes of faults in elastic solids. *Journal of Geophysical Research: Solid Earth*, *100*(B7), 12959-12983. doi: 10.1029/94JB03037

Ben-Zion, Y., & Rice, J. R. (1997). Dynamic simulations of slip on a smooth fault in an elastic solid. *Journal of Geophysical Research: Solid Earth*, *102*(B8), 17771-17784. doi: 10.1029/97JB01341

Burridge, R., & Knopoff, L. (1967). Model and theoretical seismicity. *Bulletin of the Seismological Society of America*, *57*(3), 341-371.

Cattania, C. (2019). Complex earthquake sequences on simple faults. *Geophysical Research Letters*, *46*(17-18), 10384-10393. doi: 10.1029/2019GL083628

Chen, T., & Lapusta, N. (2009). Scaling of small repeating earthquakes explained by interaction of seismic and aseismic slip in a rate and state fault model. *Journal of Geophysical Research*, *114*. doi: 10.1029/2008JB005749

Cochard, A., & Madariaga, R. (1994). Dynamic faulting under rate-dependent friction. *Pure and Applied Geophysics*, *142*, 419-445. doi: 10.1007/BF00876049

Day, S. M., Dalguer, L. A., Lapusta, N., & Liu, Y.   (2005).   Comparison of finite difference and boundary integral solutions to three-dimensional spontaneous rupture. *Journal of Geophysical Research: Solid Earth*, *110*(B12). doi: 10.1029/2005JB003813

Di Toro, G., Han, R., Hirose, T., De Paola, N., Nielsen, S., Mizoguchi, K., . . . Shi-

mamoto, T.   (2011, mar).   Fault lubrication during earthquakes.   *Nature*, *471*, 494.

Dieterich, J. H.   (1979).   Modeling of rock friction 1. experimental results and constitutive equations. *Journal of Geophysical Research*, *84*(B5), 2161-2168.

Douilly, R., Aochi, H., Calais, E., & Freed, A. M.   (2015).   Three-dimensional dynamic rupture simulations across interacting faults: The Mw 7.0, 2010, Haiti earthquake.   *Journal of Geophysical Research: Solid Earth*, *120*(2), 1108-1128. doi: 10.1002/2014JB011595

Duan, B., & Oglesby, D. D.   (2006).   Heterogeneous fault stresses from previous earthquakes and the effect on dynamics of parallel strike-slip faults.   *Journal of Geophysical Research: Solid Earth*, *111*(B5). doi: 10.1029/2005JB004138

Dunham, E. M., Belanger, D., Cong, L., & Kozdon, J. E.   (2011a).   Earthquake ruptures with strongly rate-weakening friction and off-fault plasticity, part 2: Nonplanar faults.   *The Bulletin of the Seismological Society of America*, *101*, 2308-2322. doi: 10.1785/0120100076

Dunham, E. M., Belanger, D., Cong, L., & Kozdon, J. E.   (2011b).   Earthquake ruptures with strongly rate-weakening friction and off-fault plasticity, part1: Planar faults.   *Bulletin of the Seismological Society of America*, *101*(5), 2296-2307. doi: 10.1785/0120100075

Erickson, B. A., & Day, S. M.   (2016).   Bimaterial effects in an earthquake cycle model using rate-and-state friction.   *Journal of Geophysical Research: Solid Earth*, *121*(4), 2480-2506. doi: 10.1002/2015JB012470

Erickson, B. A., & Dunham, E. M.   (2014).   An efficient numerical method for earthquake cycles in heterogeneous media: Alternating subbasin and surface-rupturing events on faults crossing a sedimentary basin. *Journal of Geophysical Research: Solid Earth*, *119*(4), 3290-3316. doi: 10.1002/2013JB010614

Erickson, B. A., Dunham, E. M., & Khosravifar, A.   (2017).   A finite difference method for off-fault plasticity throughout the earthquake cycle.   *Journal of the*

Mechanics and Physics of Solids, *109*, 50 - 77.   doi: https://doi.org/10.1016/
j.jmps.2017.08.002

Erickson, B. A., Jiang, J., Barall, M., Lapusta, N., Dunham, E. M., Harris, R., . . .
Wei, M.   (2020).   The Community Code Verification Exercise for Simulating
Sequences of Earthquakes and Aseismic Slip (SEAS).   *Seismological Research
Letters*, *91*(2A), 874–890. doi: 10.1785/0220190248

Field, E. H. (2019). How Physics Based Earthquake Simulators Might Help Improve
Earthquake Forecasts. *Seismological Research Letters*, *90*(2A), 467-472. doi: 10
.1785/0220180299

Field, E. H., Biasi, G., Bird, P., Dawson, T., Felzer, K.R., . . . Zeng, Y.   (2013).
Uniform California Earthquake Rupture Forecast, version 3 (UCERF3)
−the time-independent model.   *U.S. Geological Survey Open-File Report
2013?1165, 97 p., California Geological Survey Special Report 228*.   doi:
http://pubs.usgs.gov/of/2013/1165/

Galvez, P., Ampuero, J.-P., Dalguer, L. A., Somala, S. N., & Nissen-Meyer, T.
(2014).   Dynamic earthquake rupture modelled with an unstructured 3-D spec-
tral element method applied to the 2011 M9 Tohoku earthquake.   *Geophysical
Journal International*, *198*(2), 1222-1240. doi: 10.1093/gji/ggu203

Harris, R., Archuleta, R. J., & Day, S. M.   (1991).   Fault steps and the dynamic
rupture process: 2-D numerical simulations of a spontaneously propagat-
ing shear fracture.   *Geophysical Research Letters*, *18*(5), 893-896.   doi:
10.1029/91GL01061

Harris, R., Barall, M., Aagaard, B., Ma, S., Roten, D., Olsen, K., . . . Dalguer, L.
(2018). A Suite of Exercises for Verifying Dynamic Earthquake Rupture Codes.
Seismological Research Letters, *89*(3), 1146-1162. doi: 10.1785/0220170222

Harris, R., Barall, M., Archuleta, R., Dunham, E., Aagaard, B., Ampuero, J. P.,
. . . Templeton, E.   (2009).   The SCEC/USGS dynamic earthquake rup-
ture code verification exercise.   *Seismological Research Letters*, *80*.   doi:

847   10.1785/gssrl.80.1.119

848   Harris, R., & Day, S. M. (1993). Dynamics of fault interaction: parallel strike-slip

849   faults. *Journal of Geophysical Research: Solid Earth*, *98*(B3), 4461-4472. doi:

850   10.1029/92JB02272

851   Harris, R., & Day, S. M. (1999). Dynamic 3D simulations of earthquakes on en ech-

852   elon faults. *Geophysical Research Letters*, *26*(14), 2089-2092. doi: 10.1029/

853   1999GL900377

854   Hu, F., Zhang, Z., & Chen, X. (2016). Investigation of earthquake jump distance for

855   strike-slip step overs based on 3-D dynamic rupture simulations in an elastic

856   half-space. *Journal of Geophysical Research: Solid Earth*, *121*(2), 994-1006.

857   doi: 10.1002/2015JB012696

858   Jiang, J., & Lapusta, N. (2016). Deeper penetration of large earthquakes on seis-

859   mically quiescent faults. *Science*, *352*(6291), 1293–1297. doi: 10.1126/science

860   .aaf1496

861   Johnson, E. (1992). The influence of the lithospheric thickness on bilateral slip. *Geo-*

862   *physical Journal International*, *108*(1), 151-160. doi: 10.1111/j.1365-246X.1992

863   .tb00846.x

864   Kame, N., Rice, J. R., & Dmowska, R. (2003). Effects of prestress state and rupture

865   velocity on dynamic fault branching. *Journal of Geophysical Research: Solid*

866   *Earth*, *108*(B5). doi: 10.1029/2002JB002189

867   Kaneko, Y., Avouac, J.-P., & Lapusta, N. (2010). Towards inferring earthquake pat-

868   terns from geodetic observations of interseismic coupling. *Nature Geoscience*,

869   *3*, 363-369. doi: 10.1038/NGEO843

870   Kaneko, Y., & Lapusta, N. (2008). Variability of earthquake nucleation in con-

871   tinuum models of rate-and-state faults and implications for aftershock rates.

872   *Journal of Geophysical Research*, *113*, B12312. doi: 10.1029/2007JB005154

873   Lambert, V., & Barbot, S. (2016). Contribution of viscoelastic flow in earthquake

874   cycles within the lithosphere-asthenosphere system. *Geophysical Research Let-*

875   *ters*, *43*(19), 10,142-10,154. doi: 10.1002/2016GL070345

876   Lambert, V., & Lapusta, N.   (2020).   Rupture-dependent breakdown energy in fault

877   models with thermo-hydro-mechanical processes.   *Solid Earth*, *11*(6), 2283–

878   2302. doi: 10.5194/se-11-2283-2020

879   Lambert, V., Lapusta, N., & Perry, S.   (2021).   Propagation of large earthquakes as

880   self-healing pulses or mild cracks.   *Nature*, *591*(7849), 252–258.   doi: 10.1038/

881   s41586-021-03248-1

882   Lapusta, N., & Liu, Y.   (2009).   Three-dimensional boundary integral modeling of

883   spontaneous earthquake sequences and aseismic slip.   *Journal of Geophysical

884   Research*, *114*, B09303. doi: 10.1029/2008JB005934

885   Lapusta, N., & Rice, J.   (2003).   Low-heat and low-stress fault operation in earth-

886   quake models of statically strong but dynamically weak faults.   *AGU FAll

887   Meeting Abstracts*.

888   Lapusta, N., Rice, J. R., Ben-Zion, Y., & Zheng, G.   (2000).   Elastodynamic analysis

889   for slow tectonic loading with spontaneous rupture episodes on faults with

890   rate- and state- dependent friction.   *Journal of Geophysical Research*, *105*,

891   765-789. doi: 10.1029/2000JB900250

892   Lehner, F. K., Li, V. C., & Rice, J. R.   (1981).   Stress diffusion along rupturing plate

893   boundaries.   *Journal of Geophysical Research: Solid Earth*, *86*(B7), 6155-6169.

894   doi: 10.1029/JB086iB07p06155

895   Lin, Y.-Y., & Lapusta, N.   (2018).   Microseismicity simulated on asperity-like fault

896   patches: On scaling of seismic moment with duration and seismological esti-

897   mates of stress drops.   *Geophysical Research Letters*, *45*(16), 8145-8155.   doi:

898   10.1029/2018GL078650

899   Liu, Y.   (2014).   Source scaling relations and along-strike segmentation of slow slip

900   events in a 3-D subduction fault model. *Journal of Geophysical Research: Solid

901   Earth*, *119*(8), 6512-6533. doi: 10.1002/2014JB011144

902   Liu, Y., & Rice, J. R.   (2005).   Aseismic slip transients emerge spontaneously

in three-dimensional rate and state modeling of subduction earthquake sequences. *Journal of Geophysical Research: Solid Earth*, *110*(B8). doi: 10.1029/2004JB003424

Liu, Y., & Rice, J. R. (2007). Spontaneous and triggered aseismic deformation transients in a subduction fault model. *Journal of Geophysical Research: Solid Earth*, *112*(B9). doi: 10.1029/2007JB004930

Lozos, J. C., Oglesby, D. D., Brune, J. N., & Olsen, K. B. (2015). Rupture and Ground-Motion Models on the Northern San Jacinto Fault, Incorporating Realistic Complexity. *Bulletin of the Seismological Society of America*, *105*(4), 1931-1946. doi: 10.1785/0120140327

Michel, S., Avouac, J.-P., Lapusta, N., & Jiang, J. (2017). Pulse-like partial ruptures and high-frequency radiation at creeping-locked transition during megathrust earthquakes. *Geophysical Research Letters*, *44*(16), 8345-8351. doi: 10.1002/2017GL074725

Noda, H., & Lapusta, N. (2010). Three-dimensional earthquake sequence simulations with evolving temperature and pore pressure due to shear heating: Effect of heterogeneous hydraulic diffusivity. *Journal of Geophysical Research*, *115*, B123414. doi: 10.1029/2010JB007780

Noda, H., & Lapusta, N. (2013). Stable creeping fault segments can become destructive as a result of dynamic weakening. *Nature*, *493*, 518 EP -.

Okubo, K., Bhat, H. S., Rougier, E., Marty, S., Schubnel, A., Lei, Z., ... Klinger, Y. (2019). Dynamics, radiation, and overall energy budget of earthquake rupture with coseismic off-fault damage. *Journal of Geophysical Research: Solid Earth*, *124*(11), 11771-11801. doi: 10.1029/2019JB017304

Olami, Z., Feder, H. J. S., & Christensen, K. (1992). Self-organized criticality in a continuous, nonconservative cellular automaton modeling earthquakes. *Phys. Rev. Lett.*, *68*, 1244–1247. doi: 10.1103/PhysRevLett.68.1244

Perrin, G., Rice, J. R., & Zheng, G. (1995). Self-healing slip pulse on a frictional

surface. *Journal of the Mechanics and Physics of Solids*, *43*(9), 1461 - 1495. doi: https://doi.org/10.1016/0022-5096(95)00036-I

Perry, S. M., Lambert, V., & Lapusta, N. (2020). Nearly magnitude-invariant stress drops in simulated crack-like earthquake sequences on rate-and-state faults with thermal pressurization of pore fluids. *Journal of Geophysical Research: Solid Earth*, *125*(3), e2019JB018597. doi: 10.1029/2019JB018597

Poliakov, A. N. B., Dmowska, R., & Rice, J. R. (2002). Dynamic shear rupture interactions with fault bends and off-axis secondary faulting. *Journal of Geophysical Research: Solid Earth*, *107*(B11), ESE 6-1-ESE 6-18. doi: 10.1029/2001JB000572

Rice, J. R. (1980). The mechanics of earthquake rupture. *in Physics of Earth's Interior*, 555-649.

Rice, J. R. (1993). Spatio-temporal complexity of slip on a fault. *Journal of Geophysical Research: Solid Earth*, *98*(B6), 9885-9907. doi: 10.1029/93JB00191

Rice, J. R. (2006). Heating and weakening of faults during earthquake slip. *Journal of Geophysical Research*, *111*, B05311. doi: 10.1029/2005JB004006

Rice, J. R., & Ben-Zion, Y. (1996, 04). Slip complexity in earthquake fault models. *Proceedings of the National Academy of Sciences of the United States of America*, *93*(9), 3811–3818. doi: 10.1073/pnas.93.9.3811

Rice, J. R., & Ruina, A. L. (1983). Stability of steady frictional slipping. *Journal of Applied Mechanics*, *50*(2), 343-349.

Richards-Dinger, K., & Dieterich, J. H. (2012). RSQSim Earthquake Simulator. *Seismological Research Letters*, *83*(6), 983-990. doi: 10.1785/0220120105

Ross, Z. E., Trugman, D. T., Hauksson, E., & Shearer, P. M. (2019). Searching for hidden earthquakes in southern california. *Science*, *364*(6442), 767–771. doi: 10.1126/science.aaw6888

Rubin, A., & Ampuero, J.-P. (2005). Earthquake nucleation on (aging) rate and state faults. *Journal of Geophysical Research: Solid Earth*, *110*(B11).

Ruina, A. (1983). Slip instability and state variable friction laws. *Journal of Geophysical Research*, *88*(B12), 10359-10370.

Segall, P., & Rice, J. R. (1995). Dilatancy, compaction, and slip instability of a fluid-infiltrated fault. *Journal of Geophysical Research: Solid Earth*, *100*(B11), 22155-22171. doi: 10.1029/95JB02403

Segall, P., Rubin, A. M., Bradley, A. M., & Rice, J. R. (2010). Dilatant strengthening as a mechanism for slow slip events. *Journal of Geophysical Research: Solid Earth*, *115*(B12). doi: 10.1029/2010JB007449

Shaw, B. E., Milner, K. R., Field, E. H., Richards-Dinger, K., Gilchrist, J. J., Dieterich, J. H., & Jordan, T. H. (2018). A physics-based earthquake simulator replicates seismic hazard statistics across california. *Science Advances*, *4*(8). doi: 10.1126/sciadv.aau0688

Sieh, K. E., Jones, L., Hauksson, E., Hudnut, K., Eberhart-Phillips, D., Heaton, T., ... Zachariasen, J. (1993). Near-field investigations of the Landers Earthquake Sequence, April to July 1992. *Science*, *260*(5105), 171–176. doi: 10.1126/science.260.5105.171

Thomas, M. Y., Lapusta, N., Noda, H., & Avouac, J.-P. (2014). Quasi-dynamic versus fully dynamic simulations of earthquakes and aseismic slip with and without enhanced coseismic weakening. *Journal of Geophysical Research*, *119*, 1986-2004. doi: 10.1002/2013JB010615

Tullis, T. (2007). Friction of rock at earthquake slip rates. *Treatise on Geophysics*, *4*, 131-152. doi: 10.1016/B978-044452748-6.00064-X

Tullis, T., Richards-Dinger, K., Barall, M., Dieterich, J. H., Field, E. H., Heien, E. M., ... Yikilmaz, M. B. (2012). Generic Earthquake Simulator. *Seismological Research Letters*, *83*(6), 959-963. doi: 10.1785/0220120093

Ulrich, T., Gabriel, A.-A., Ampuero, J.-P., & Xu, W. (2019). Dynamic viability of the 2016 Mw 7.8 Kaikoura earthquake cascade on weak crustal faults. *Nature Communications*, *10*(1), 1213. doi: 10.1038/s41467-019-09125-w

Wei, S., Helmberger, D., & Avouac, J.-P. (2013). Modeling the 2012 Wharton basin earthquakes off-Sumatra: Complete lithospheric failure. *Journal of Geophysical Research: Solid Earth*, *118*(7), 3592-3609. doi: 10.1002/jgrb.50267

Withers, K. B., Olsen, K. B., Day, S. M., & Shi, Z. (2018). Ground Motion and Intraevent Variability from 3D Deterministic Broadband (0-7.5 Hz) Simulations along a Nonplanar Strike-Slip Fault. *Bulletin of the Seismological Society of America*, *109*(1), 229-250. doi: 10.1785/0120180006

Wollherr, S., Gabriel, A.-A., & Mai, P. M. (2019). Landers 1992 reloaded: Integrative dynamic earthquake rupture modeling. *Journal of Geophysical Research: Solid Earth*, *124*(7), 6666-6702. doi: 10.1029/2018JB016355

Wu, Y., & Chen, X. (2014). The scale-dependent slip pattern for a uniform fault model obeying the rate- and state-dependent friction law. *Journal of Geophysical Research: Solid Earth*, *119*(6), 4890-4906. doi: 10.1002/2013JB010779

Ye, L., Lay, T., Kanamori, H., & Rivera, L. (2016). Rupture characteristics of major and great (Mw > 7.0) megathrust earthquakes from 1990 to 2015: 2. depth dependence. *Journal of Geophysical Research: Solid Earth*, *121*(2), 845-863. doi: 10.1002/2015JB012427

Supporting Information for "Resolving simulated sequences of earthquakes and fault interactions: implications for physics-based seismic hazard assessment"

Valère Lambert[1] and Nadia Lapusta[1,2]

[1]Seismological Laboratory, California Institute of Technology, Pasadena, California, USA

[2]Department of Mechanical and Civil Engineering, California Institute of Technology, Pasadena, California, USA

Contents of this file

1. Text S1

2. Figures S1 to S9

Text S1: Description of initial shear stress distributions for numerical simulations of long-term sequences of earthquakes and aseismic slip.

In our simulations of sequences of earthquakes and aseismic slip (SEAS), the distributions of shear stress and slip along the fault evolve depending upon the history of previous slip during periods of rapid seismic slip as well as slow aseismic slip and fault locking. We consider how the long-term evolution of fault slip differs among simulations using varying computational cell sizes and considerations of inertial effects, given the same initial conditions for shear stress, slip rate and the rate-and-state frictional state variable θ.

For all of our simulations, the velocity-strengthening (VS) portions of the fault are set to be initially creeping at steady state with the prescribed tectonic plate rate of $V_{ini} = V_{pl}$:

April 1, 2021, 3:52pm

$$\tau_{VS}^{\text{ini}} = \tau_{\text{ss}}(V_{\text{pl}}) = \overline{\sigma} \left[f_* + (a_{\text{VS}} - b_{\text{VS}}) \ln \frac{V_{\text{pl}}}{V_*} \right] \tag{1}$$

$$\tau_B^{\text{ini}} = \tau_{\text{ss}}(V_{\text{pl}}) = \overline{\sigma} \left[f_* + (a_{\text{B}} - b_{\text{B}}) \ln \frac{V_{\text{pl}}}{V_*} \right] \tag{2}$$

21 For points within the velocity-weakening (VW) segments of the fault, we first consider the

22 initial shear stress distribution $S1$, which favors the first rupture nucleating along the VW-VS

23 boundary around $x = 33$ km and then jumping across the VS barrier to produce a two-segment

24 rupture (e.g. Figure 2 of the main text) :

$$\tau_{VW}^{\text{ini}}(x) = \begin{cases} \tau_{\text{ss}}(1 \text{ m/s}) + 3.5\text{MPa} & \text{for} \quad x \in [-33\text{km}, -2\text{km}) \\ \tau_{\text{ss}}(V_{\text{pl}}) + a_{VW} \ln \frac{0.1\text{m/s}}{V_{\text{pl}}} - 1.5\text{MPa} & \text{for} \quad x \in [-2\text{km}, -1\text{km}) \\ \tau_{\text{ss}}(1 \text{ m/s}) + 5\text{MPa} & \text{for} \quad x \in (1\text{km}, 27\text{km}) \\ \tau_{\text{ss}}(V_{\text{pl}}) + a_{VW} \ln \frac{0.1\text{m/s}}{V_{\text{pl}}} & \text{for} \quad x \in [27\text{km}, 33\text{km}] \end{cases} \tag{3}$$

25 In all of our simulations, points with the VW segments are initially locked with initial slip rate

26 $V_{\text{ini}} = 10^{-10}$ m/s and the initial state variable θ chosen to be consistent with the corresponding

27 initial shear stress and slip rate, given equation 2 in the main text.

28

29 In order to examine the convergence of long-term sequences of earthquakes with different

30 initial conditions, we consider a second initial shear stress distribution $S2$ (Figures 3A vs B in

31 the main text), which favors the first rupture nucleating near the VS barrier around $x = 1$ km

32 and propagating away from the barrier and spanning the entire right VW segment:

$$\tau_{VW}^{\text{ini}}(x) = \begin{cases} \tau_{\text{ss}}(1 \text{ m/s}) + 3.5\text{MPa} & \text{for} \quad x \in [-33\text{km}, -1\text{km}) \\ \tau_{\text{ss}}(V_{\text{pl}}) + a_{VW} \ln \frac{0.1\text{m/s}}{V_{\text{pl}}} & \text{for} \quad x \in (1\text{km}, 7\text{km}] \\ \tau_{\text{ss}}(1 \text{ m/s}) + 5\text{MPa} & \text{for} \quad x \in (7\text{km}, 33\text{km}] \end{cases} \tag{4}$$
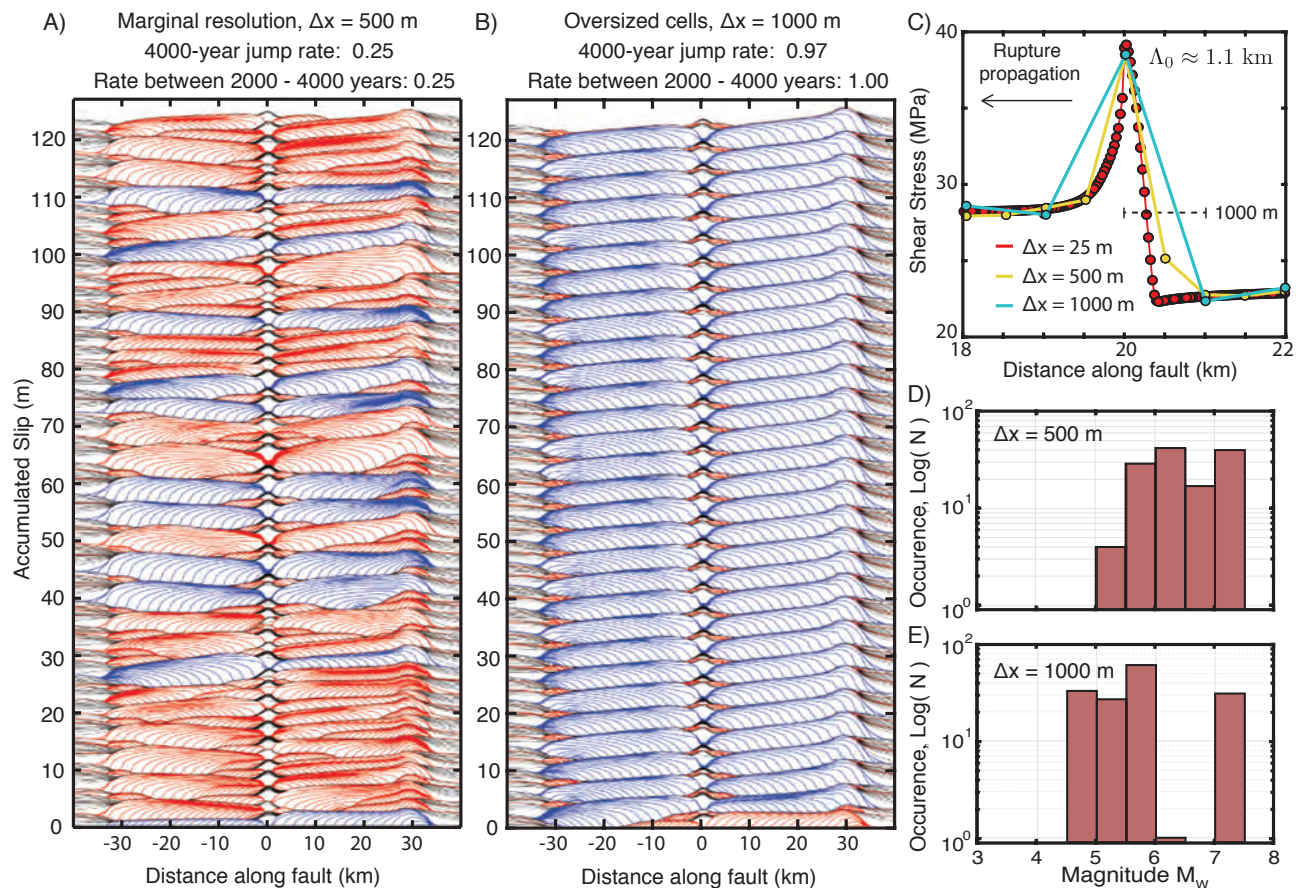
Figure S1. Inadequately-resolved simulations of fault model M1 exhibiting different simulated earthquake sequences and rates of two-segment ruptures. (A-B) History of cumulative slip over 4000 years in fully dynamic simulations of fault model M1 using oversized cells of (A) 500 m and (B) 1000 m, respectively. Contours of seismic slip are plotted every 0.5 s, with ruptures that jump across the VS barrier colored blue. (C) Spatial distribution of shear stress around the rupture front in a well-resolved simulation ($\Delta x = 25$ m, red) and the two simulations with oversized cells ($\Delta x = 500$ and 1000 m). As the cell size increases, the breakdown of shear stress at the rupture front is increasingly poorly resolved. (D-E) Frequency-magnitude histograms for events in (A-B), respectively. Simulations with oversized cells exhibit different long-term sequences of events compared to the well-resolved simulations (Figure 2 of main text), with increased production of small events and significantly different rates of two-segment ruptures.

April 1, 2021, 3:52pm
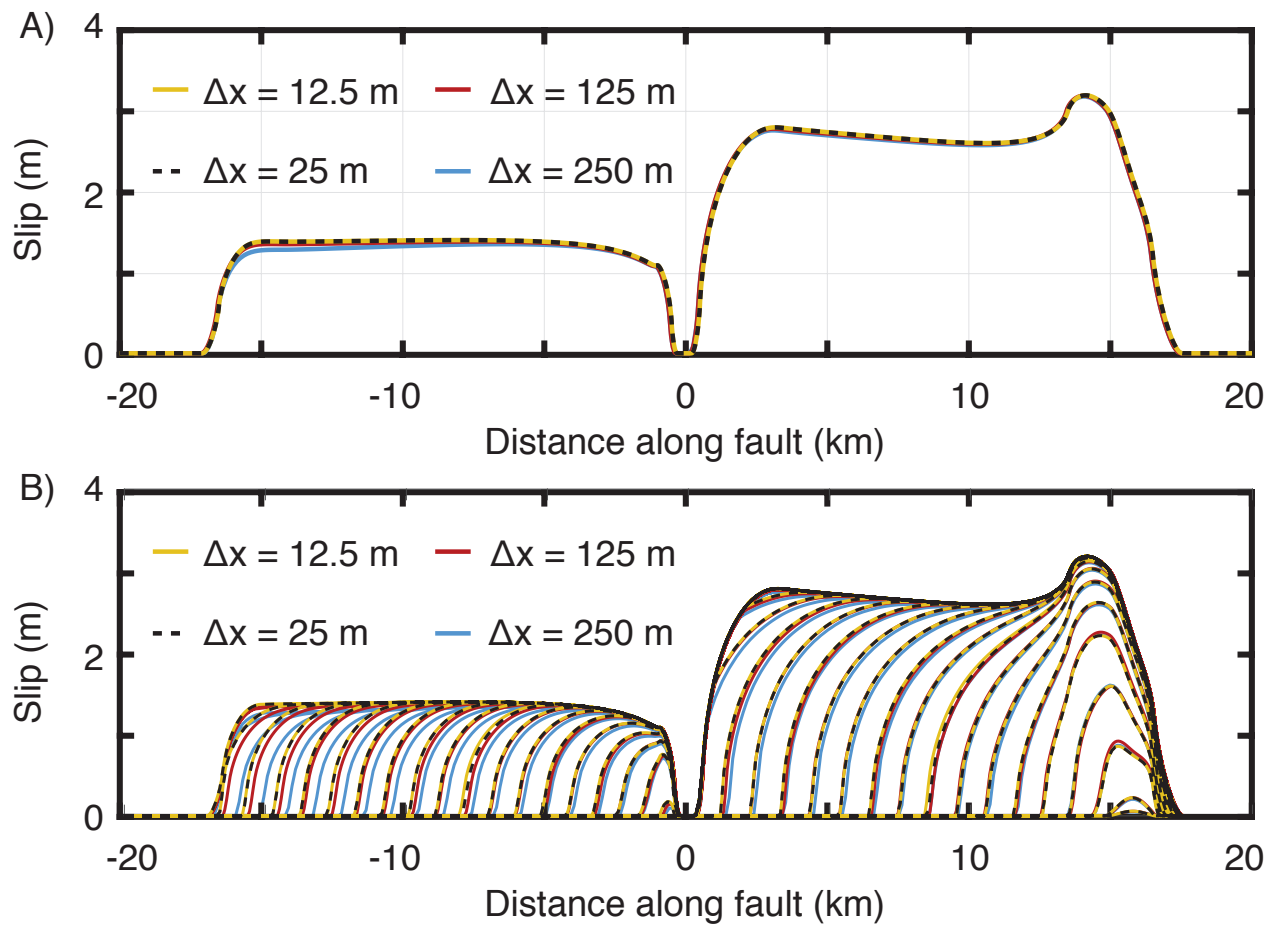
Figure S2. Final slip and evolution of slip for the first rupture in simulations of fault model M1 with different numerical resolution. (A) The final slip distribution for the first simulated rupture with the same initial conditions is practically the same for simulations using cell sizes of 12.5, 25, 125 and 250 m. (B) The evolution of slip is contoured every 0.5 s and comparable spacing between contours illustrates that the rupture speed is generally consistent for the first rupture in these well-resolved and marginally-resolved simulations. The evolution of slip and final slip are virtually identical for the two well-resolved simulations using 12.5 and 25 m cells and the average final slip for simulations with 12.5 and 250 m cell sizes differ by less than 0.8%.
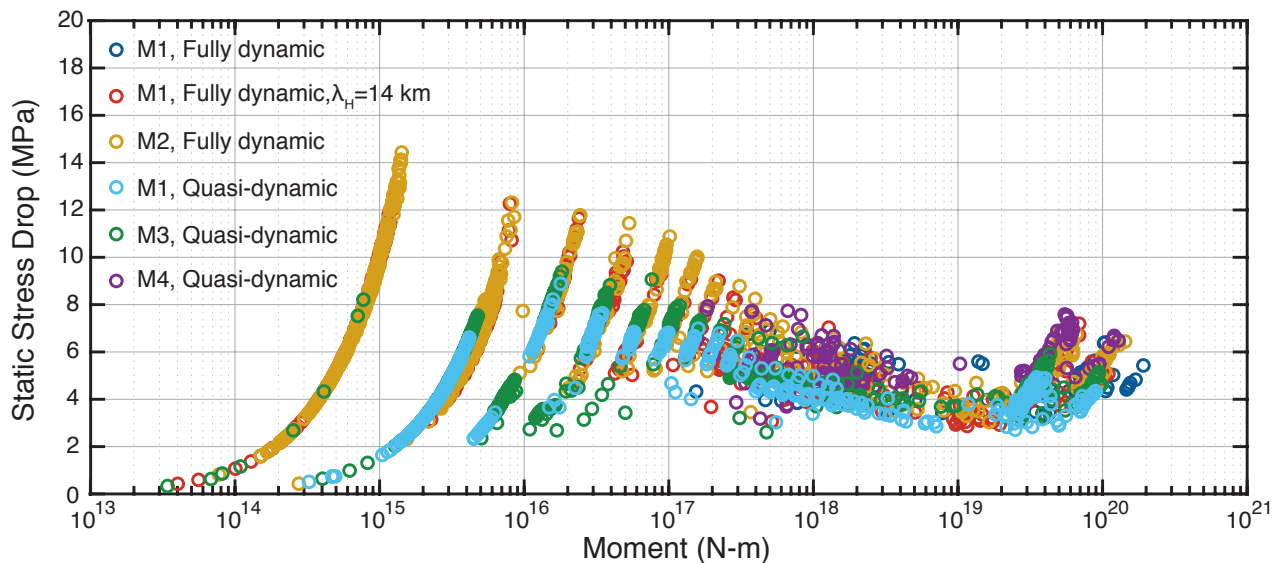
Figure S3. Comparable scaling of average static stress drop versus moment with reasonable stress drop values between 1 to 10 MPa for simulated ruptures in the six sets of simulations shown in Figure 9 of the main text. The six models all use oversized cells of $\Delta x = 1000$ m and produce comparable earthquake frequency-magnitude statistics.
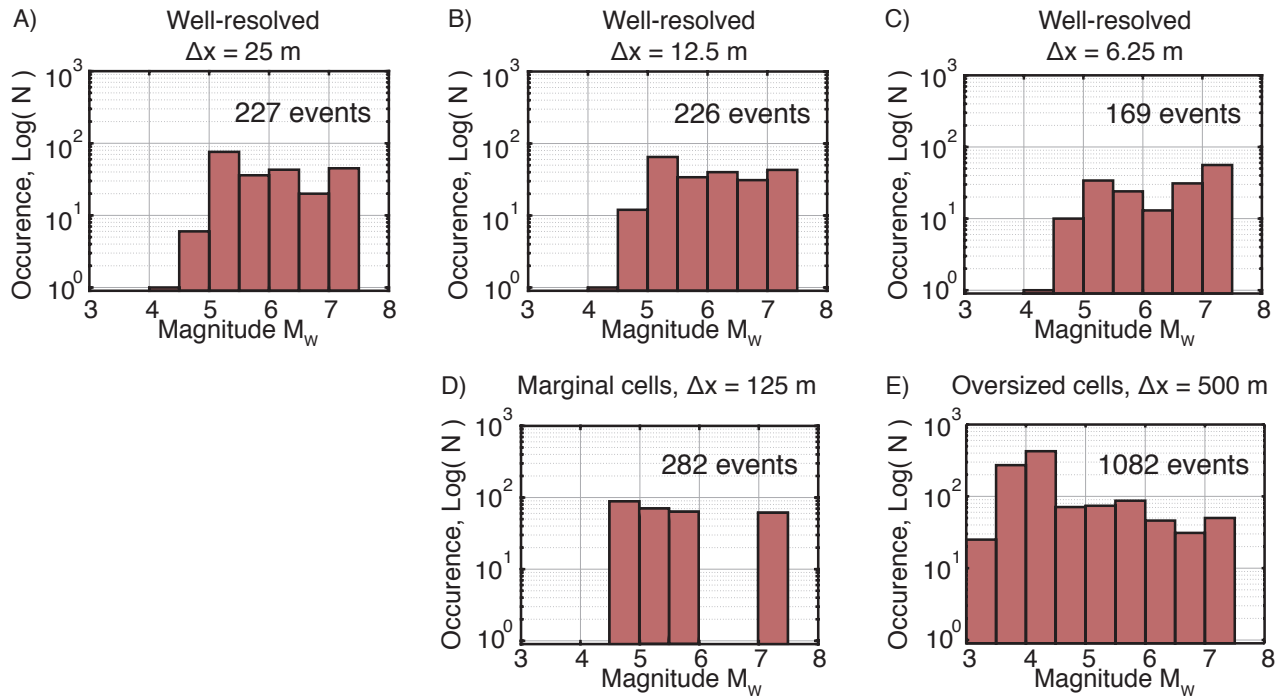
Figure S4.   Differing frequency-magnitude histograms for 4000 years of sequences of earth-quakes in fully dynamic simulations of fault model M5 with varying cell sizes. Simulations are performed using different computational cell sizes of (A) 25 m, (B) 12.5 m, (C) 6.25 m, (D) 125 m and (E) 500 m. Simulations exhibit differences in long-term behavior, even for well-resolved simulations (A-C) where the stress at the rupture front is spatially described by more than 3 cells. Simulations using oversized cells or with marginal resolution (D & E) produce more smaller events as small groups of cells nucleate into ruptures that fail to propagate due to the stress concentration at the rupture front being poorly resolved.
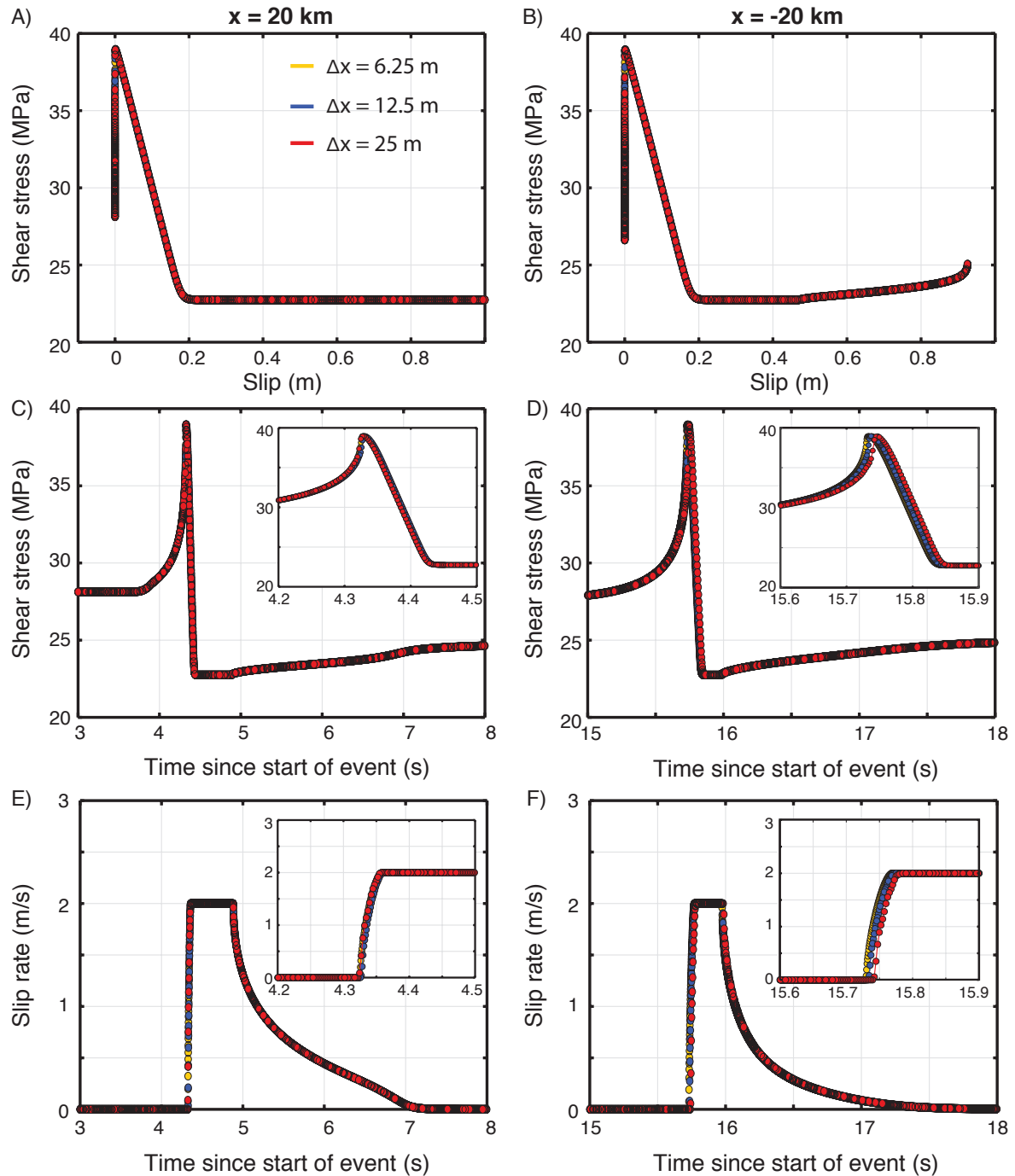
Figure S5. Evolution of local slip rate and shear stress with slip and time at two points at (left) $x = 20$ km and (right) $x = -20$ km during the first rupture of adequately-discretized fully dynamic simulations of fault model M5 with the effects of off-fault dissipation approximated using a velocity limit of $V_{\text{lim}} = 2$ m/s, as shown in Figure 17 of main text. The local behavior is nearly identical for all three simulations with different spatial discretization.
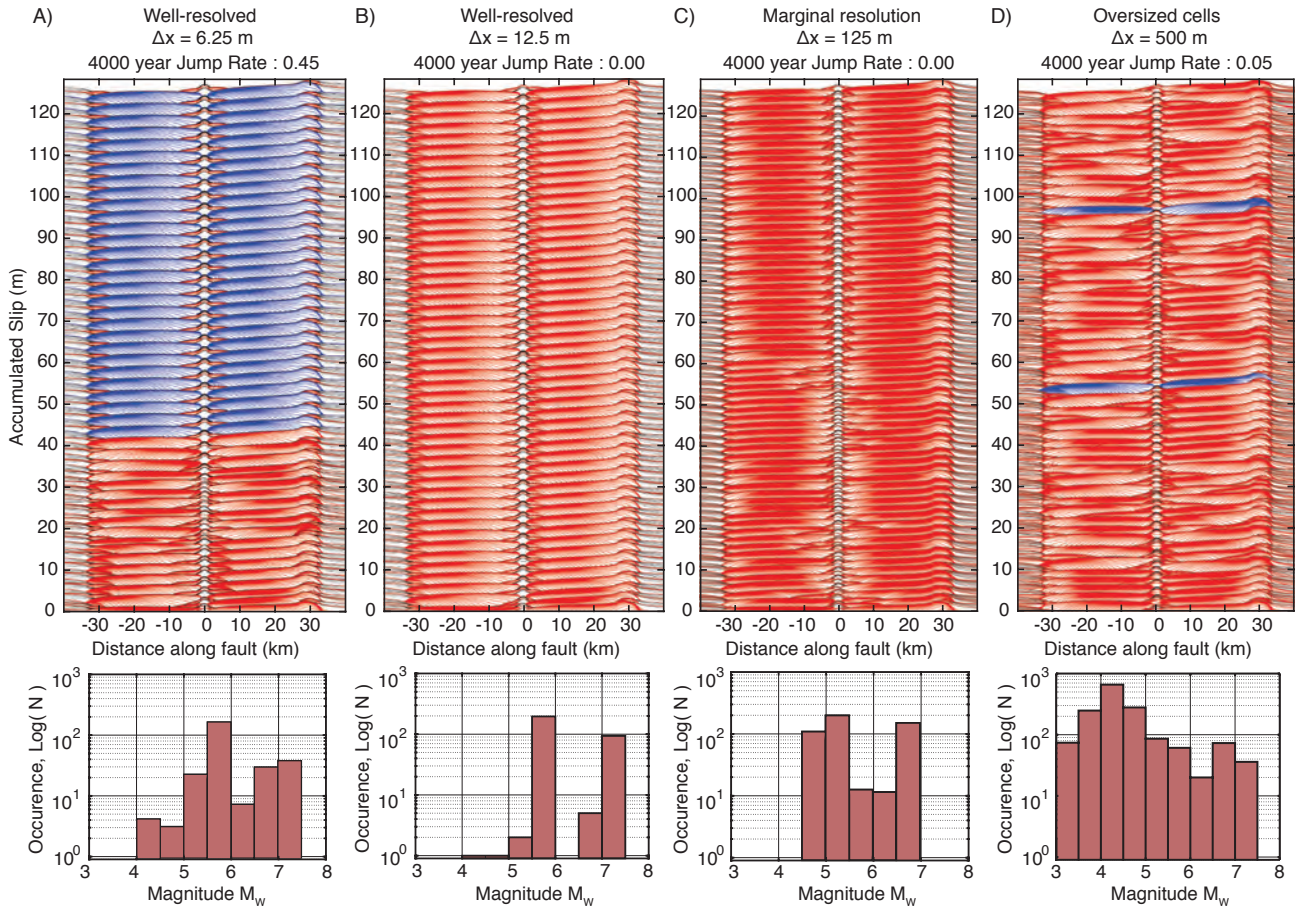
Figure S6. Different sequences of earthquakes and rate of two-segment ruptures over 4000 years in quasi-dynamic simulations with different resolution of fault model M5. (Top) Slip history for simulations with varying spatial resolution showing different histories of events depending on the choice of cell size. Seismic slip is contoured every 0.5 s with ruptures jumping across the VS barrier colored blue. (Bottom) Frequency-magnitude statistics for the respective simulations of varying cell size shown above. Simulations using larger cell sizes produce a larger number of small events as small groups of cells nucleate but ruptures cannot propagate due to the inadequately resolved stress concentration at the rupture front. Even adequately-resolved simulations show different histories of events, including rates of ruptures jumping across the VS barrier.
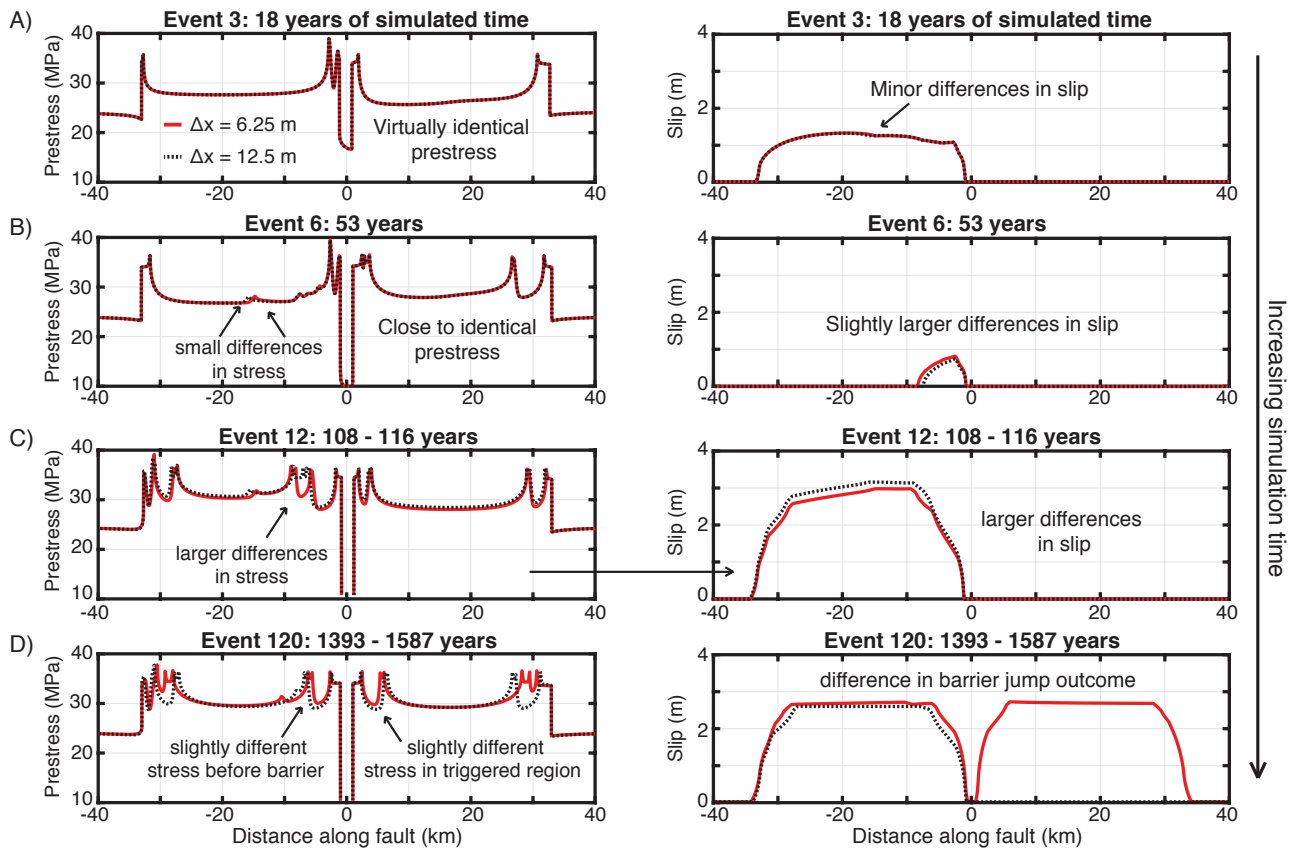
Figure S7. Compounded effects of small numerical differences in well-resolved quasi-dynamic simulations result in diverging long-term earthquake sequences. Comparison of prestress before rupture (left) and resulting slip distributions (right) for several events over the first 2000 years of simulated time in two quasi-dynamic simulations of fault model M5 using cell sizes of 6.25 m (red) and 12.5 m (black). (A & B) The evolution of shear stress and accumulated slip during the first few sequences of events is practically identical, however small differences begin to appear due to different numerical approximations. (C) The small differences in shear stress accumulate over sequences of events, resulting in more noticeable variations in the amount of slip in larger events. (D) The accumulation of noticeable differences in shear stress, particularly in regions of rupture nucleation and near the VS barrier, leads to differing sequences of events, rupture sizes, and probabilities of rupture jumping across the VS barrier.
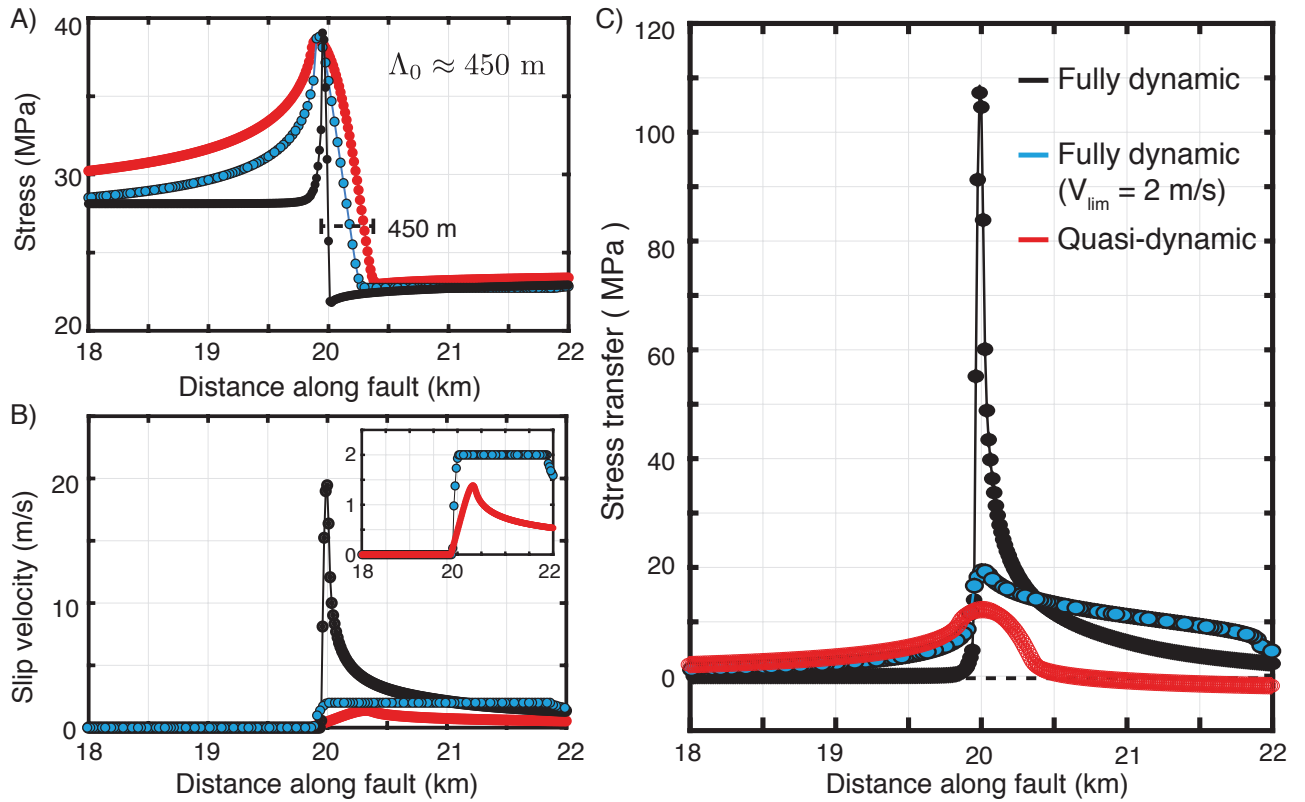
Figure S8. Comparison of local slip rate, shear stress and stress transfer with different treatment of inertial effects and considerations for plasticity. (A-B) Spatial distribution of (A) shear stress, (B) slip rate and (C) stress transfer along the fault during the first rupture with the same initial conditions in fully dynamic (black) and quasi-dynamic (red) simulations of fault model M5, as well as a fully dynamic simulation approximating the effects of off-fault plasticity with a slip velocity limit of 2 m/s. The stress transfer during fully dynamic ruptures is much more pronounced than quasi-dynamic ruptures, resulting in higher slip rates and more focused shear stresses at the rupture front. The approximation for off-fault plasticity limits the peak slip velocity and restricts the magnitude of the peak stress transfer along the fault. However, the stress transfer for the fully dynamic rupture including the plasticity approximation is still more pronounced than that of the quasi-dynamic rupture and remains more pronounced behind the rupture front.
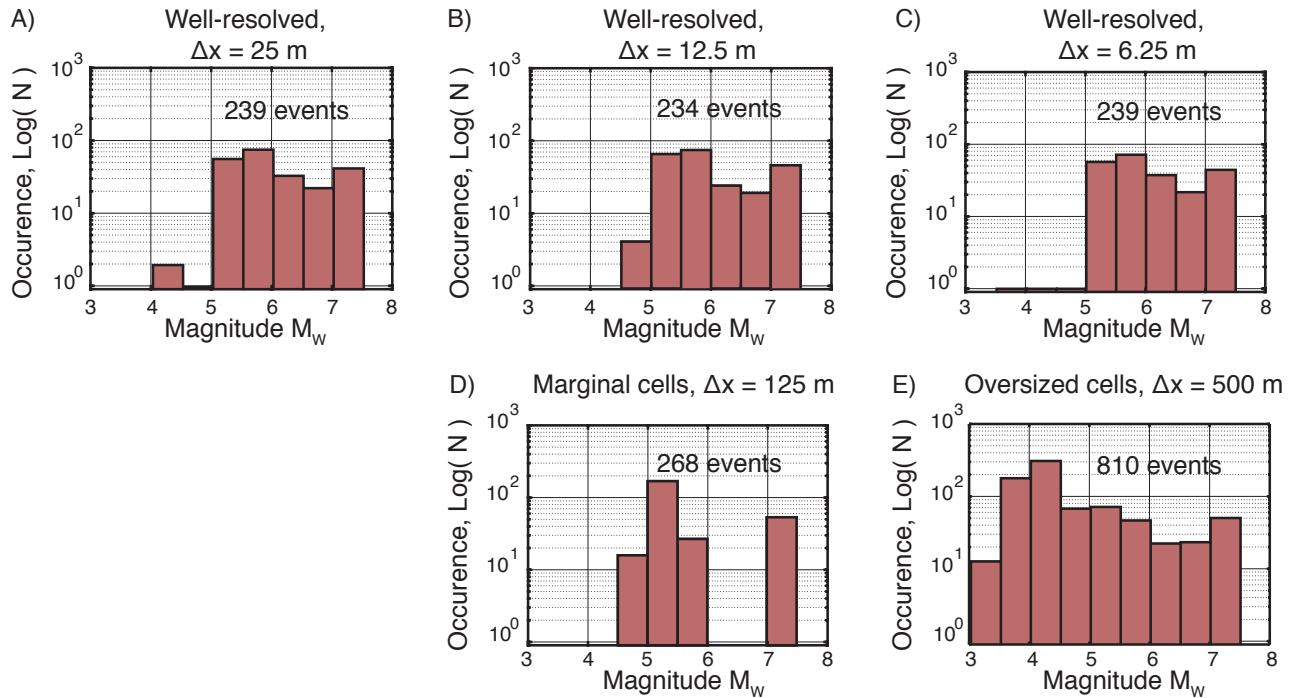
Figure S9. Frequency-magnitude histograms for 4000 years of sequences of earthquakes in fully dynamic simulations of fault model M5 with the effects of off-fault dissipation approximated using a slip velocity limit of $V_{\mathrm{lim}} = 2$ m/s. Simulations are performed using different computational cell sizes of (A) 25 m, (B) 12.5 m, (C) 6.25 m, (D) 125 m and (E) 500 m. The increased production of smaller events ($M_{\mathrm{w}} \leq 4$) in simulations with large computations cells (D & E) is qualitatively similar to the fully dynamic simulations of fault model M5 with no velocity limit shown in Figure S4.